POLITECNICO DI MILANO

Industrial Engineering Faculty

Space Engineering Degree

Use of the Statistical Energy Analysis for dynamic predictions at satellite level

Supervisor: Prof. Ing. Sergio RICCI

Degree thesis of:

Emanuele BLASI   Matr. 719855

Considerate la vostra semenza:
fatti non foste a viver come bruti,
ma per seguir virtute e canoscenza

Consider ye the seed from which ye sprang:
ye were not made to live like unto brutes,
but for pursuit of virtue and of knowledge

Considérez votre dignité d'homme:
vous n'avez pas été appelés à vivre comme la brute,
mais vous devez acquérir de la gloire et de sublimes connaissances

— Dante Alighieri
Divina Commedia, Inferno XXVI

To my parents

ABSTRACT

The Statistical Energy Analysis (sᴇᴀ) is an efficient analysis for time calculation to predict the responses in medium and high frequencies. It may be an alternative to ꜰᴇᴍ methods. The training course will start with a bibliographical review of the sᴇᴀ, to popularise the method and to determine the limits and the advantages compared to other methods. The theory will be used to develop a Matlab code, the last one will be used on simple cases for different types of excitations (sine and acoustics) and compared with usual results.

Key words: Statistical Energy Analysis, sᴇᴀ, sᴇᴀ-Like, Quasi-sᴇᴀ, medium frequecies, high frequencies, micro vibrations, acoustic, acceleration, satellite, dynamic, prediction.

SOMMARIO

Il Statistical Energy Analysis (sᴇᴀ) è un'analisi efficiente per la predizione della risposta dinamica di una struttura nelle medie/alte frequenze. Esso può essere un'alternativa al metodo ad elementi finiti (ꜰᴇᴍ). Il progetto parte con una ricerca bibliografica al fine di inquadrare il metodo e determinarne i limiti ed i vantaggi. Dalla teoria verrà sviluppato un codice Matlab che verrà applicato su alcuni semplici modelli, i risultati così ottenuti saranno comparati con quelli usuali.

Parole chiave: Statistical Energy Analysis, sᴇᴀ, sᴇᴀ-Like, Quasi-sᴇᴀ, medie frequenze, alte frequenze, micro vibrazioni, acustica, accelerazione, satellite, dinamica, predizione.

ACKNOWLEDGEMENTS

CONTENTS

LIST OF FIGURES

INTRODUCTION

In the ambit of a continuous research to improve satellites performance, the need of high frequency analysis appears. The dynamic analysis of a complex structure is carried out by Nastran that can guarantee good results as far as $100 - 150\,\text{Hz}$. In fact, starting by $150\,\text{Hz}$, the temporal step necessary for the analysis becomes very small and implies a heavier calculation. Moreover, the modal density increases so the solution becomes confusing. The high frequency analysis is interesting in order to know the interaction between the gyroscope and the payload during the operational life. The knowledge of these interactions allows to know also the more sensible parts of the structure and where make adjustments to increase the performances. It is in this context that the Statistical Energy Analysis (SEA) comes into play.

This report describes the basic concepts of the SEA method and presents its application to structures. The first part is composed by a bibliography research to give the necessary basic knowledge for a correct development of the following phases. In this first phase the characteristics of the SEA method were identified and summarized in the chapter 1, however, for a complete overview of the subject a deeper study of the bibliography is suggested. Then, following the needs of Astrium and the description of the three principal SEA methods (Classic SEA, Quasi-SEA or SEA-Like and Energy Flow Method), the Quasi-SEA method was chosen and described in chapter 2.

Following, a Matlab code able to analyze a system (such as a satellite) was developed. A first simple model was developed to validate the code, to understand the parameters of the Quasi-SEA and to know the influence of the principal elements of the analysis (chapter 3).

But, the most interesting phase of the study is the evaluation of the acceleration in the system by the parameters of the SEA (chapter 4). Three methods of evaluation of the acceleration were developed for different purposes, such as, a quick estimation of the acceleration average, study of the hypothesis of the SEA and participation of the modes in the SEA analysis. Different analyses were developed to understand the influence of the parameters of the system and of the FE model.

In the final chapter all the hypothesis and results obtained on previous analyses were applied to a more complex model. Nevertheless, other studies are necessary, due to the appearence of a different SEA's behavior.

With this report an extensive analysis of the SEA method was done for a better learning of the hidden aspects on both theory and scientific articles. The objective of the report is to be a guide to apply the SEA not only at acoustic level but also on the study of microvibrations, and also to be a first trace for a correct study of the model/system to analyze.

The author advised and apologize for the possible presence of errors in the drafting of the report.

1 | SEA METHOD

CONTENTS

In this chapter a general presentation of the SEA method will be shown. Moreover, the hypothesis necessary to apply the method and all the elements who characterized it will be listed. Finally, a short description of the different types of analyses and methods and the interests who promote the SEA will be given. This chapter gives a rapid overview of the SEA method, hence, for a better comprehension, the lecture of [10, 16, 17] is suggested.

1.1 INTRODUCTION

SEA was originally developed by Lyon in the 1960s for the analysis of random vibrations of complex structural and fluid systems [15]. According to Lyon [17], SEA has been described as a point of viewin dealing with vibration of complex structures, and as such it employs a series of analytical and experimental methods, most of which pre-date the identification of SEA The view-point is statistical because the systems under analysis are presumed to be drawn from populations with random parameters; energy is the independent dynamical variable chosen because, by using it, distinctions between acoustical and mechanical systems disappear; and analysis emphasizes that SEA is an approach to problems rather than a set of techniques as such.

In SEA, a complex structure is required to be divided into several simple, identifiable mechanical and/or acoustical subsystems. The behavior
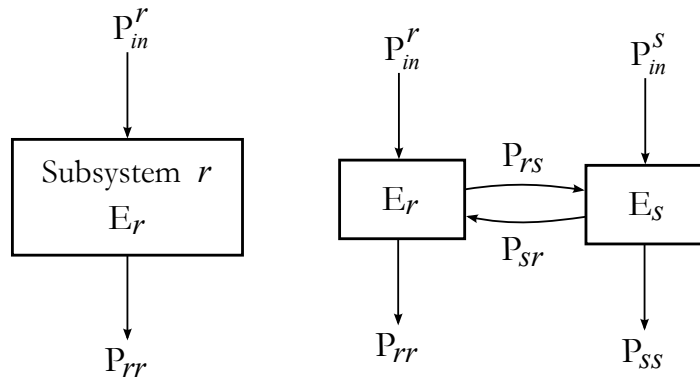
Figure 1: Partition of a system, **left:** a single subsystem; **right:** coupled subsystems

of each subsystem is characterized in a statistical sense. By solving the energy balance equations which involve the expressions for the power flowing from one subsystem to another, the distribution of the vibration energy among these coupled subsystems can be estimated. Since the time and spatial averaged vibration energy of each subsystem is normally the primary variable in SEA, SEA is not able to describe the vibration details inside each subsystem. Nevertheless, in noise and vibration control engineering, such statistical results are sufficient in most cases to quantify vibro-acoustics effects, especially at high frequencies.

Since the day that SEA was developed, applications of SEA in scientific research and engineering have drawn great attention within the noise and vibration community. So far, it has been widely used in analyzing the sound transmission in buildings, noise and vibration distributions in large scale structures, such as aircrafts, ships, vehicles, and the noise radiated from machinery structures, and so on. SEA has already been proven to be an effective approach dealing with the vibration and acoustics problems of complex structures.

1.2 STATISTICAL ENERGY ANALYSIS

Consider a single subsystem, a separated part of the structure that is to be analysed. Any excitation acting on the subsystem can be characterised by the resulting power input $P_{in}^{(r)}$ into the subsystem (Fig. 1, left). If power is injected, the subsystem stores vibrational energy E_r. In practice, there
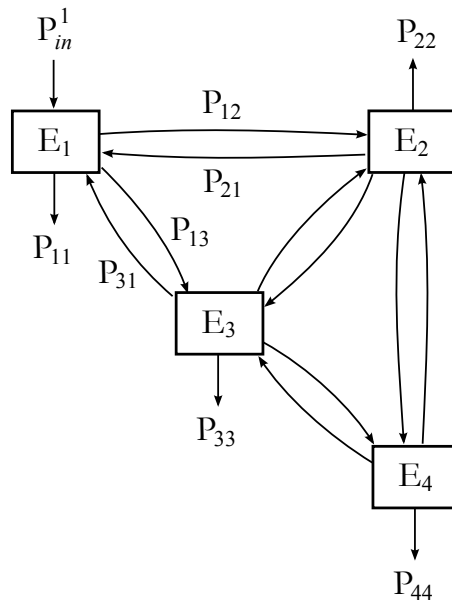
Figure 2: Example of four coupled subsystems

will be also a power loss P_{rr} (e.g. due to dissipation). This power loss may be related to the stored energy by the damping loss factor η_r by:

$$P_{rr} = \omega \eta_r E_r \qquad (1.1)$$

Further, if the analysis is restricted to steady state, it is clear that power input equals power loss: $P_{in}^{(r)} = P_{rr}$.

Consider now a second subsystem (Fig. 1, right). If this subsystem were coupled to the first, the same power balance would hold for both subsystems r and s, respectively. As a result of the coupling the subsystems share their vibrational energies. Power flows from subsystem r to subsystem s. From the viewpoint of subsystem r, this power flow P_{rs} is a power loss. A power flow exists also in the reverse direction (P_{sr}) that is as a result a power gain for subsystem s. To characterise these power flows, a special quantity, the coupling loss factor η_{rs} , is used in SEA. It is defined similarly to the damping loss factor in Eq. 1.1:

$$P_{rs} = \omega \eta_{rs} E_s \qquad (1.2)$$

In Figure 2, the case of four subsystems is shown as an example. This time, there is only a power input to subsystem 1. This power input is equal to the sum power losses (due to dissipation and coupling) for that

subsystem minus the power gains coming from the subsystems 2 and 3. The power balance reads then:

$$P_1 = P_{11} + P_{12} + P_{13} - P_{21} - P_{31} \tag{1.3}$$

Similar power balances may be established for the remaining subsystems:

$$0 = P_{22} + P_{21} + P_{23} + P_{24} - P_{12} - P_{32} - P_{42}$$
$$0 = P_{33} + P_{31} + P_{32} + P_{34} - P_{13} - P_{23} - P_{43} \tag{1.4}$$
$$0 = P_{44} + P_{42} + P_{43} - P_{24} - P_{34}$$

As there is no power input into these subsystems, the left hand side vanishes in the equations. The power quantities in Eq. 1.3 and 1.4 may be substituted by the damping and coupling loss factors and the vibrational energy as in Eq. 1.1 and 1.2. The resulting equations may then be written down together as a system of equations:

$$\begin{Bmatrix} P_1 \\ 0 \\ 0 \\ 0 \end{Bmatrix} = \omega \begin{bmatrix} \eta_{11} & -\eta_{21} & -\eta_{31} & -\eta_{41} \\ -\eta_{12} & \eta_{22} & -\eta_{32} & -\eta_{42} \\ -\eta_{13} & -\eta_{23} & \eta_{33} & -\eta_{43} \\ -\eta_{14} & -\eta_{24} & -\eta_{34} & \eta_{44} \end{bmatrix} \begin{Bmatrix} E_1 \\ E_2 \\ E_3 \\ E_4 \end{Bmatrix} \tag{1.5}$$

$$\mathbf{P_{in}} = \mathbf{LE} \tag{1.6}$$

In the example, subsystems 1 and 4 are not coupled and consequently the corresponding coupling loss factors are zero. The diagonal elements of the loss factor matrix in 1.5 are called the total loss factors as they are the sum of all coupling loss factors that are associated with power losses for the respective subsystem:

$$\eta_{rr} = \eta_r + \sum_{s, s \neq r} \eta_{rs}. \tag{1.7}$$

1.3 MODAL OVERLAP M_r

The modal overlap of a subsystem is defined as

$$M_r = \omega \eta_r n_r \tag{1.8}$$

Where n_r is the modal density, it is defined as the number of modes per unit frequency interval. Physically, the modal overlap denotes the average number of modes lying within a typical modal half power bandwidth. A high modal overlap factor means that neighboring resonance peaks largely merge together, giving a high probability for a system to be characterized as resonant, which is essential to SEA applications. Generally, it is assumed that a system with its subsystem modal overlap factors less than unity is not amenable to an SEA approach. However, one should be clear that the actual number of modes being excited within a system depends on the initial condition of the excitations, not the modal overlap. [6]

1.4 TYPES OF ANALYSES

Depending on the characteristics of the matrix **L** there are three types of analyses (the classical SEA analysis, the quasi-SEA or SEA-like analysis, and the energy flow analysis) all of which fall in the scope of Eq. 1.6 but have different valid conditions and governing territories, were summarized in [19]:

- The *classical* SEA only considers resonant transmissions between directly coupled subsystems. No indirect coupling paths exist in the model. All the power flow are reciprocal, and thus matrix **L** is symmetric with the elements being loss factors as defined in Eq. 1.6 and 1.7. The coupling loss factors and internal loss factors are positive with their physical significances as defined.

- *Quasi*-SEA or SEA-*like* analysis includes direct coupling paths and indirect coupling paths as well because the requirements for the classical SEA analysis are not being fully satisfied. The reciprocity relationship is still valid for all power flow paths, indicating that only resonant transmissions, either direct or indirect, are considered. Thus matrix **L** is still symmetric. However, negative loss factors might occur in the model due to the equivalencies in the parameters caused by the substructuring scheme that is not fully compliant with the physical nature of the power flow topology within the system.

- The *Energy Flow Analysis* basically includes all the power transmission paths, not only the resonant but also the no-resonant transmissions, in the model. Thus matrix **L** is generally full and not

necessarily symmetrical, indicating that there is no reciprocity relationship in the system. The elements in the coupling matrix are generally energy flow coefficients and could be positive or negative.

1.5 TYPES OF METHODS

A great number of methods that circumvent some of these limitations and problems have been developed, but up to now only on an academic level. The following list gives an (incomplete) overview together with the main idea behind each method [24]:

- *Wave Intensity Analysis* (WIA) [12]: like SEA, but fourier decomposition of wave field intensity in a subsystem - relaxes the diffuse field assumption of SEA;

- *Energy Finite Element Method* (EFEM) [22]: analogy with heat conduction;

- (*Integral*) *Smooth Energy Model* (SEM) [14] or *High Frequency Boundary Element Method* (HFBEM): boundary integral formulation using energy variables;

- *Energetic Mean Mobility Approach* (EMMA) [23]: suited for treatment of heterogenous structures, especially for experimental application;

- *Complex Envelope Distribution Analysis* (CEDA) [4]: analysis using a cepstrum calculated from wavenumber spectrum rather than from frequency spectrum (not energy-based);

- *Hybrid Methods*: incorporate explicit "modal" behaviour of components into SEA-like models, e.g. [13].

1.6 ADVANTAGES OF SEA

- It requires only a relative coarse design of the physical system with relatively few parameters.

- It uses few degrees of freedom per subsystem.

- The use of SEA model allows an analyst to retain a "feel" for the behaviour of the system in terms of the physical influence of system parameters. Because the latter are few in number, and computer runs are very cheap and quick, SEA is very useful in early design exercises.

- SEA is based on the principle of conservation of energy, and violations of this principle can easily be detected. Also, an assumption of equipartition of modal energy between a directly-excited and non-directly-excited subsystem provides an estimate of the response of the latter with prior knowledge of only the order of magnitude of the transfer coefficient and damping. Alternatively it provides a conservative estimate of the upper limit of the response.

1.7 APPLICATIONS IN ENGINEERING

The SEA models could be used to define or refine the vibroacoustic behaviour of a system both in the first part of the design and during the product's life. Below, a little description of the principal possible analyses [1] can be found.

- *Determination of the energetic response*: knowing the input power in each subsystem the energetic response is obtained. These values can be used to draw the vibroacoustic velocity and the component's acceleration or the pressure in the acoustic cavity. If the values aren't acceptable, these data allow applying some operations to reduce the vibrations or the noise in the components.

- *Localize the sources*: knowing the energie in each subsystem the power is obtained then, the potions of the sources. Using this data it is possible to act on the sources directly to eliminate the undesired effects.

- *Identification of energy flows*: by the resolution of the SEA model it is easy to find and classify, in order of importance, the path of transmission of the energy. So, it is possible to act on the subsystem to reduce the transmission through the most important path.

- *Sensibility analysis*: this analysis allows the identification of the most important parameters that contribute to the response of a subsystem. Then, it is possible to know which parameters to change to obtain the best refinement.

2 | QUASI–SEA METHOD

This chapter will explain the Quasi-SEA method. Moreover, the hypothesis necessary to apply this method will be depicted for a good comprehension of its limits of usage. Each element of the theory will be analysed in order to give a general knowledge of the topic [19–21].

2.1 ENERGY DISTRIBUTION AND SEA MODEL

The system is divided into subsystems which are excited by random, stationary, distributed forces. It is assumed that the system is linear and that the excitations applied to the different subsystems are uncorrelated. The response is described by the time-average input powers $\mathbf{P_{in}}$ and the subsystem energies $\mathbf{E}$ averaged over some frequency band Ω.

2.1.1 ED model and SEA matrices

In an energy distriubution (ED) model the energies and input power are related by

$$\mathbf{E} = \mathbf{A}\mathbf{P_{in}} \tag{2.1}$$

where $\mathbf{A}$ is a matrix of energy influence coefficients in the relevant frequency band. The element $\mathbf{A_{rs}}$ gives the (time and frequency average) energy in subsystem r per unit (time and frequency average) power input to subsystem s. $\mathbf{A}$ is not symmetric, although symmetry exists regarding the modal energies in some circumstances.

If an energy distriubution model is formed, then Eq. 2.1 can be inverted to give

$$P_{in} = XE; \quad X = A^{-1} \tag{2.2}$$

Ideally, X is a proper SEA matrix and its elements satisfy both the necessary and the desirable conditions described above. However, this need not be the case for two reasons. Firstly, X describes the response of a single system over a specific frequency band and thus normally differs from the ensemble average (e.g., finite number of modes, specific details of those modes, etc.). Secondly, the SEA assumptions and approximations may be invalid or inaccurate. The result is that the elements of X may not satisfy all the necessary or desirable conditions of a proper-SEA or an Quasi-SEA model even when ensemble averaged. For example, X may not satisfy the consistency relations, in which case X is not Quasi-SEA.

Expressions for the energy distriubution matrix A are found from the modal properties of the system. This requires only the assumptions of linearity and uncorrelated excitations, although various other simplifying assumptions are made for convenience. The conditions under which an SEA model can be formed are then examined. It is seen that, under some mild conditions (primarily that there are enough, *typical* modes in the band), the matrix X is an Quasi-SEA matrix, but it need not be a proper-SEA matrix: it satisfies all the necessary conditions of an SEA matrix but need not satisfy the desirable conditions.

2.1.2 Energy influece coefficients

Expressions for the energy influence coefficients are derived in terms of the modes of the system. Proportional, viscous damping is assumed, although the modes may have different bandwidths. The system modes are assumed to be mass normalized so that

$$\int \rho(x)\phi_j(x)\phi_k(x)\,dx = \delta_{jk} \tag{2.3}$$

where $\rho(x)$ is the mass density.

The total kinetic energy can be found by integrating the kinetic energy density over the whole system. From the orthogonality relations (Eq. 2.3), it follows that, for each mode j,

$$P_{in,j} = 2\Delta_j T_j \tag{2.4}$$

where T_j is the kinetic energy in mode j. This is of course merely a statement of conservation of energy, mode by mode. Subsequently, the total energy will be approximated by twice the kinetic energy, the time average kinetic energy and the time average potential energy are equal. The viscous damping has been assumed with $\Delta_j = 2\zeta_j\omega_j = \eta_j\omega_j$ being the half-power modal bandwidth and ζ_j the damping factor. Proportional damping is assumed, although ζ_j may vary from mode to mode, and thus in effect be frequency dependent.

The energy influece coefficient A_{rs} is given by

$$A_{rs} = \frac{E^{(r)}}{P_{in}^{(s)}} = \frac{2T^{(r)}}{P_{in}^{(s)}} = \frac{\sum_j \sum_k \Gamma_{jk}\psi_{jk}^{(s)}\psi_{jk}^{(r)}}{\sum_j \Delta_j \Gamma_{jj}\psi_{jj}^{(s)}} \tag{2.5}$$

where the subscripts j and k refer to the jth and k^{th} modes of the system, where $T^{(r)}$ is the total kinetic energy in subsystem r and is given by

$$T^{(r)} = 2S_f \sum_j \sum_k \Gamma_{jk}\psi_{jk}^{(s)}\psi_{jk}^{(r)} \tag{2.6}$$

$S_f = S_f(\omega)$ is the spectral density, it is potentially frequency dependent, but is henceforth assumed to be constant for convenience; $P_{in}^{(s)}$ is the power input into subsystem s and is given by

$$P_{in}^{(s)} = 2S_f \sum_j 2\Delta_j \Gamma_{jj}\psi_{jj}^{(s)} \tag{2.7}$$

while Γ_{jk} is cross modal power given by

$$\Gamma_{jk}(\omega) = \frac{1}{\Omega} \int_{\omega\in\Omega} \frac{1}{4}\omega^2\beta_{jk}(\omega)\,d\omega \tag{2.8}$$

and $\psi_{jk}^{(r)}$ is cross-mode participation factor given by

$$\psi_{jk}^{(r)} = \int_{x\in r} \rho(x)\phi_j\phi_k\,dx \tag{2.9}$$

where ϕ_j is the mode shape of the jth system mode and

$$\beta_{jk}(\omega) = Re\{\alpha_j(\omega)\alpha_k(\omega)^*\} \tag{2.10}$$

dependent by modal receptance

$$\alpha(\omega) = \frac{1}{\omega_j^2 - \omega^2 + i\Delta_j\omega}. \tag{2.11}$$

For a system the following relations hold good

$$\sum_r \psi_{jj}^{(r)} = 1$$
$$\sum_r \psi_{jk}^{(r)} = 0. \tag{2.12}$$

2.1.3 Frequency integral Γ_{jk}

The cross-modal term Γ_{jk} is a frequency integral whose magnitude depends primarily on the natural frequencies of the two modes and how close are these natural frequencies. Cross-modal terms for which Γ_{jk} is large may contribute strongly to the total response. Generally, Γ_{jk} is small unless both modes j and k are resonant, i.e. unless their natural frequencies lie in Ω ($\omega_j \in \Omega$, $\omega_k \in \Omega$). The term is particularly large if the modes *overlap*, i.e., they lie within each others half-power bandwidths such that $|\omega_j - \omega_k| \leqslant (\Delta_j - \Delta_k)/2$. The self-term Γ_{jj} is always large if mode j is resonant.

Analytic expression for the integrals exist [18], but these will not be repeated here. The largest terms arise from resonant mode-pairs (especially overlapping pairs). For these, the limits of the integration can be extended to $(0, \infty)$ a good approximation.

If the damping is small, then for resonant modes the frequency integrals can be approximated by

$$\Gamma_{jj} = \frac{1}{\Omega}\frac{\pi}{8\Delta_j}$$
$$\Gamma_{jk} = \frac{1}{\Omega}\frac{\pi}{16[(\omega_j^2 - \omega_k^2)^2 + (\Delta_j\omega_j + \Delta_k\omega_k)^2]} \tag{2.13}$$

These expressions are exact if the limits of integration are $(0, \infty)$, whatever the level of damping.

2.2 OTHERS MODELS

Other models were developed to obtain the internal loss factor η_{rs} but they are slower than the method illustrated. In fact, it is necessary to excite each subsystem in sequential way and to calculate the energy E_r. Thus, knowing P_{in} and E_r it is possible to obtain η [3, 9].

3 | CODE DEVELOPMENT

CONTENTS

This chapter will introduce the most important passages to evaluate the sea characteristics. Subsequently, a critical analysis of the results will be developed to validate the code obtained by the method explained in § 2.1.

3.1 ENERGY AND FLOW POWER ESTIMATION

To validate the code and to understand the different physical characteristics of the sea, a simple model was developed. A hollow cube with the 5th surface blocked in four points. By the geometry of the model, the system was divided in six subsystems coincident to the six surfaces.
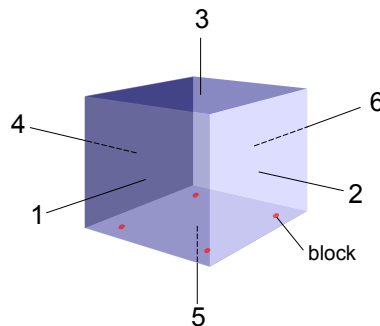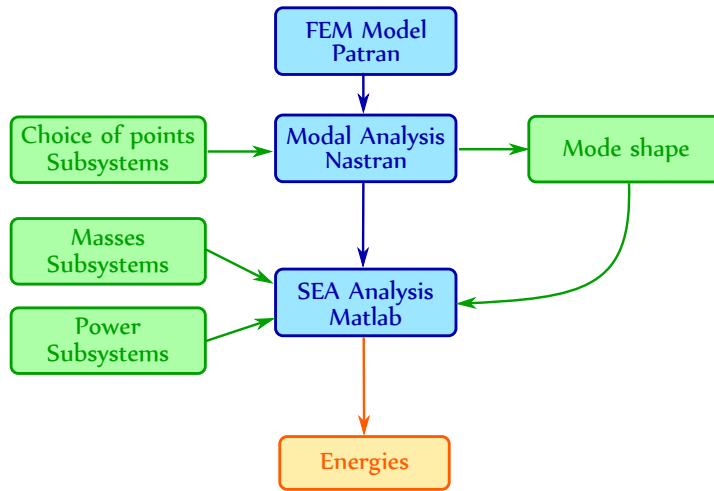

Figure 3: cube model

Figure 4: Block scheme, energies of the subsystems

The evaluation of the mode shape ϕ_j of the system is necessary to calculate the cross-mode participation factor ψ_{jk} (Eq. 2.9) and then the energy and power for the energy influence factor A_{rs} (Eq. 2.5). Starting with a FEM model of the system it was possible to obtain the mode shape by the SOL 103 resolution of Nastran. Others variables must be defined to solve the Quasi-SEA: the real mass of each subsystem, the power injected and in which subsystem and the subsystems' nodes of the fem model. A realistic value of power injected is not important to validate the code, so a symbolic power of $1\,W$ in the 5th subsystem was chosen.

3.1.1 Energy

Starting with Eq. 2.1, the subsystem energy is calculated. In Fig. 5a it is possible to observe the energy's trend for the different subsystems. We immediately notice that the energy of the 5th subsystem is larger than in the others, in accord with the power injected. Furthermore, the energy of the four lateral surfaces are obviously equal.

A second model of the cube was analyzed to observe the influence of an element not completely connected to the others. In particular, the 3rd surface, opposite to 5th, was connected to the near surfaces by 4 bolts for each edge. The bolts were designed in Nastran with the element RBE2 where the rotations aren't blocked (DOF 4, 5 and 6). By the comparison between the results shown in Fig. 5, we can observe an augmentation of
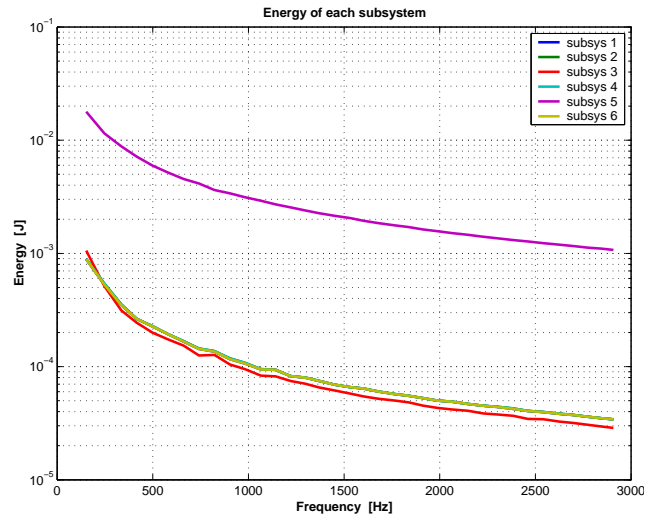
(a) First model
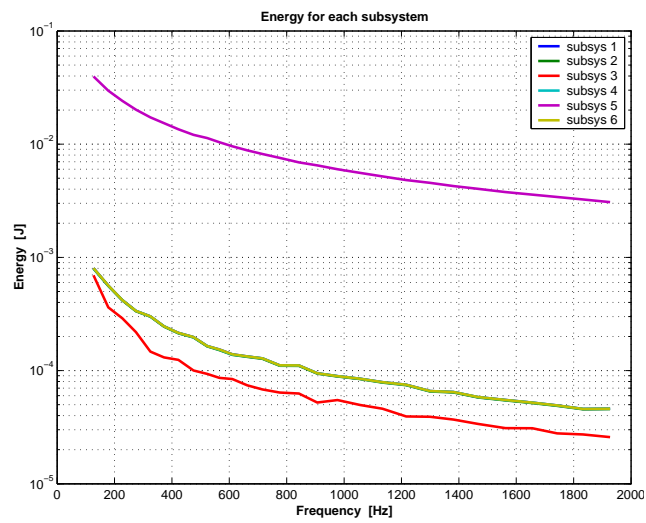
(b) Second model

Figure 5: Energies of the subsystems for the two models of cube
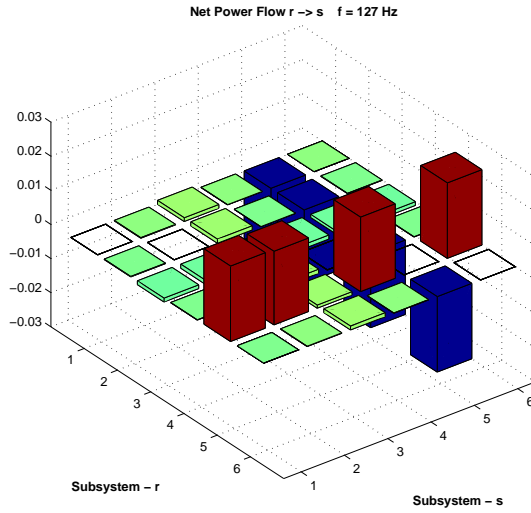
Figure 6: Net power flows

the energy of the 5th subsystem whereas the energy of the 3rd subsystem decreases due a weaker connection.

3.1.2 Net Flow Power

Knowing the energy of the subsystems and the apparent coupling loss factor, the net flow power can be easily calculated by Eq. 1.2:

$$\overline{P}_{rs} = -\overline{P}_{sr} = P_{rs} - P_{sr} \tag{3.1}$$

An overall representation of the net power flow is shown in Fig. 6. When the net power flow connected to the 3rd subsystem is negative (Fig. 7a), the net power re-enter in the subsystem. The net power flow $\overline{P}_{35}$ is not stable because the power between these two subsystems is strongly dependent on coupling modes. Whereas, the net power flow of the 5th subsystem is positive (Fig. 7b), this means that the net power exits and, in particular, an equal power enters in the four subsystems directly connected. As previously said in § 1.5, the power flows are indicative but they allow, anyway, to observe the relation between the subsystems.

It is possible to note a power flow between the 5th and the 3rd subsystem. The existence of a non-zero indirect coupling loss factor η_{rt} does not imply that energy flows between subsystems r and t (which are not physically coupled). Instead, it means that the coupling power P_{rs} between two
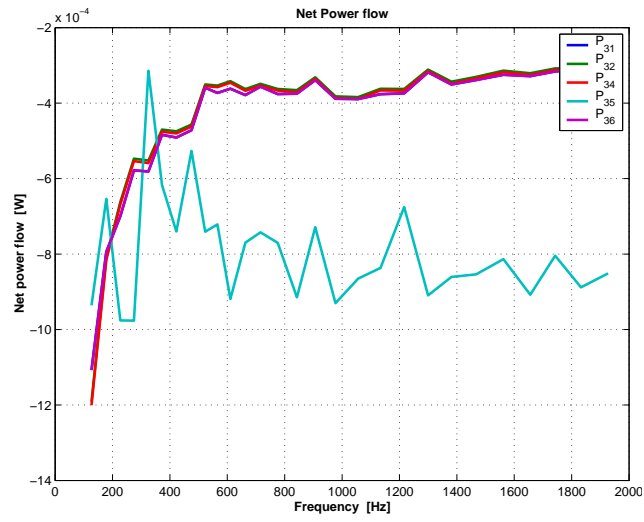
(a) $\overline{P}_{3r}$: 3rd subsystem
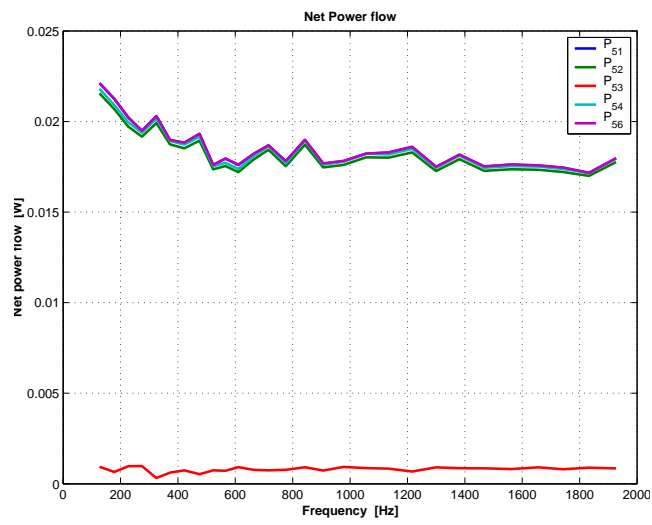
(b) $\overline{P}_{5r}$: 5th subsystem

Figure 7: Net flow power of the subsystems 3 and 5

subsystems r and s which are physically coupled depends also on the energy of the third subsystem t. Hence the SEA assumption of coupling power proportionality does not hold. The existence of indirect coupling loss factors thus indicates that some of the assumptions of conventional SEA breakdown [20].

3.2 INFLUENCE FACTORS

The solution obtained by Quasi-SEA is influenced by three factors:

- Dimension of the mesh;

- Number of points for each subsystem;

- Number of modes for each frequency band.

This section will describe the analysis and the considerations of the three factors. These factors will be analysed separately for a good comprehension of their level influence and to give the bases for a critical choice in the analysis of the system/model. To understand the influence of these factors, the simple model of the hollow cube was analysed. Moreover, different thicknesses and materials were considered to observe possible influences in the solution. In particular, there is a strong instability of the solution when a panel/subsystem is thinner than the others and with a smaller Young's module, e.g. in ratio 1/7.

3.2.1 Dimension of the mesh

Four equal systems with a different mesh are considered to observe the influence of meshing. In particular, each edge is divided into 5, 10, 20 and 40 parts then 36, 121, 441, 1681 nodes for each surface or subsystem. It is necessary to calculate the participation factor ψ_{jk} (Eq. 2.9) to resolve the Quasi-SEA method, and the participation factors need the resolution of an integral on the subsystem. Therefore, all nodes are considered to make a good comparison of the solutions of the four systems. Moreover, to obtain a valid solution with the Quasi-SEA, a modal overlap factor bigger than 1 must be guaranteed ($M > 1$, Eq. 1.8). The mesh with 5 nodes for each edge doesn't guarantee this condition.

The energy in each frequency range of the first subsystem is considered to compare the solution. It is possible to see in Fig. 8 that the solution with 5 nodes derivates from the others, while the solutions with 10, 20
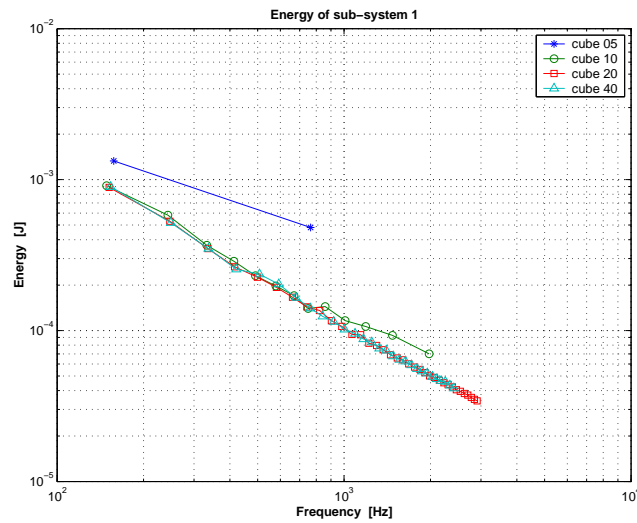
Figure 8: Energy of the subsystem 1 for different mesh

and 40 nodes are equal in all frequency bands. The solution with 10 nodes has an error after 800Hz.

For an analysis between 100 and 1000 Hz, a maximal pace of 0.075 m is necessary to guarantee an error within 10%. Whereas, for an analysis to 3000 Hz a maximal pace of 0.05 m is suggested.

3.2.2 Number of points

Because a complete analysis with all nodes is extremely heavy to calculate, different solutions of the same system, with smaller number of points are considered to find an optimal compromise between results and calculation time. Consequently, the solutions with 4, 6, 8, 10, 12, 14 points for each sub-system are considered and compared with the complete solution (400 points).

The participation factors ψ_{jk} are calculated with the hypothesis that each point participates in the same way, and with the same weight in the resolution of the integral.[1] When two points that are near to each other are chosen, the result isn't as currect as when the points are more spread apart in the mesh.

A random method is used to choose the points in the subsystems. It is interesting to see that with only 4 points it's possible to obtain the order of magnitude of the solution (Fig. 9). However, it is necessary to have a

---

1 $\psi_{jk}^{(r)} = \frac{M^{(r)}}{N^{(r)}} \sum_n^N \phi_j(x_n)\phi_k(x_n)$, where $M^{(r)}$ is the mass and $N^{(r)}$ the number of points chosen in the subsystem r
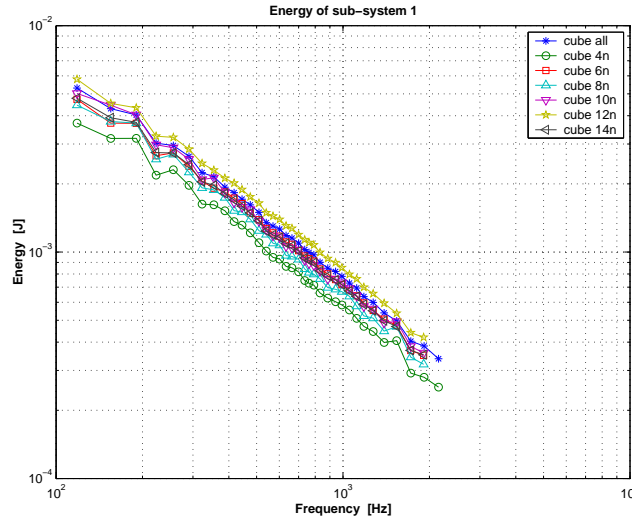
Figure 9: Energy of the subsystem 1 for different number of points

number of equal to or greater than 8 to obtain the solution nearest to the ideal case. Furthermore, $14 \, \mathrm{points/m^2}$ are needed.

3.2.3 Number of modes

A minimum number of modes is necessary to guarantee an optimal value of ψ_{jk} [7, 19]. Indeed, the solution varies in function of the number of modes considered and converges to a limit solution (Fig. 10). It is possible to have an acceptable solution with 35 modes per band. Nevertheless, too many modes are not suggested because the band becomes too large to characterize the subsystems. It is important to observe that while the energy of the subsystems changes, the total energy of the system is always constant for any number of modes considered. A changing of the energy level depends by a different number of modes considered in each band. In fact, the factor $\Gamma_{jk}\psi_{jk}^{(s)}\psi_{jk}^{(r)}$ in the evaluation of energy is not constant for any number of modes.

3.2.4 Considerations

The following combination is suggested to obtain the solution nearest to the ideal case (thin mesh, all points and perfect number of modes considered):
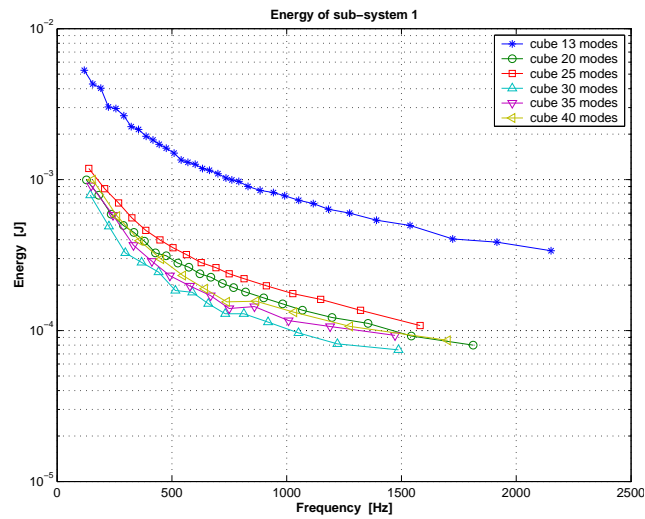
Figure 10: Energy of the subsystem 1 for different number of modes

- Pace $h \leqslant 0.075$ for an analysis to $1000\,\text{Hz}$, $h \leqslant 0.05$ for an analysis to $3000\,\text{Hz}$;

- At least $14 - 17\,\text{points}/\text{m}^2$;

- At least $10\,\text{modes per band}$ but no more of 40.

Nevertheless, there isn't a general rule for the choice of these factors. Thus, a solution very near to the ideal case or correct can't be guaranteed.

3.3 THE NANOSAT MODEL

The method was applied to a simple satellite model: Nanosat. This satellite consists of a principal structure "caisson" upon which a smaller structure "appareil" is blocked in four points. Moreover, two solar panels (panneaux) are connected to the principal structure. A graphic representation of Nanosat and the numeration of the subsystems is showed in Figure 11.

To use the SEA method, an input power of $1\,\text{W}$ is injected in the first subsystem. Analysing the results (Fig. 12 on page 27) it is possible to observe that the energy of the panels is bigger than in the other subsystems, whereas the energy of the first subsystem is the smallest. The small value of energy in the first subsystem is due to material characteristics and block conditions. Knowing that the energy is proportional to the quadratic velocity, it is easy to understand the high value of energy for
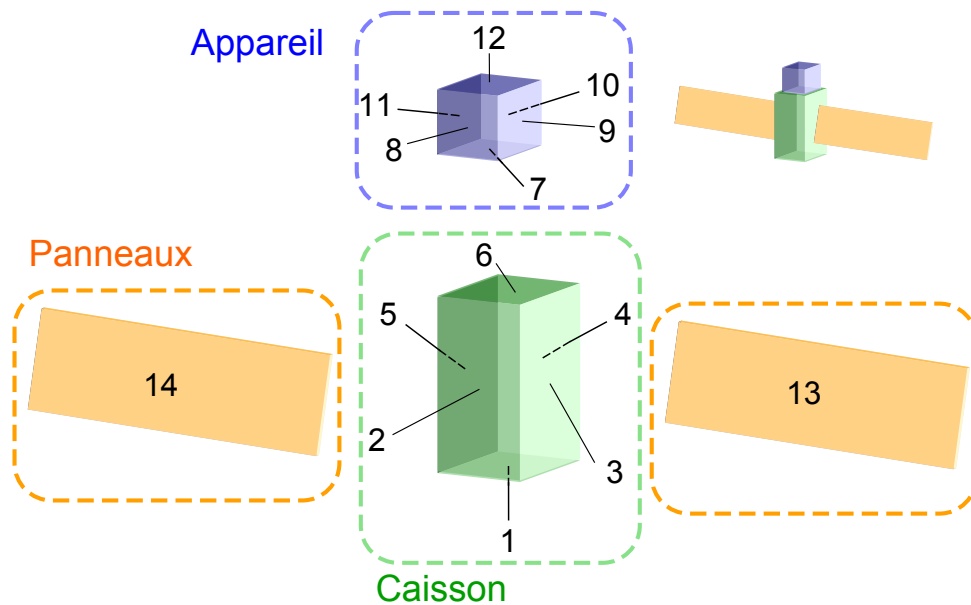
Figure 11: Nanosat model

the panels. In fact, the displacements and the mass of the panels are bigger than the other subsystems. Moreover, the fact that the energy of the panels is the same can be explained by the symmetry of the modes.

Observing the net power flows (Fig. 13), we can notice immediately an important flow at lower frequency (f = 157 Hz) between the first subsystem and the seventh. That means, a flow between the subsystem stimulated and the subsystem of the appareil blocked to the caisson, two subsystems not directly connected. A value of net power flow on the seventh subsystem higher than on the sixth subsystem could be explained by a higher mobility. This value decreases with the frequency but it can not be neglected. Moreover, the flows between the subsystems are strongly influenced by the local behaviour, this explains the difference between the values of two different bands. At high frequency a strong separation between the elements is more visible than at low frequency. In fact, at frequency of about 1850 Hz the net power flows are concentrated in the caisson, whereas at 160 Hz they are more allocated. In either case, the contribution of the caisson is more important than the other elements (appareil and panneux). The net power flows to the panels depends on the principal structure (caisson) in all bands and in particular on the subsystem connected directly (subsystem 3 for the panel 13 and subsystem 5 for the panel 14). It is interesting to observe that the net power flow between the panneaux and the appareil are not important, and the two elements are dynamically disconnected each other.
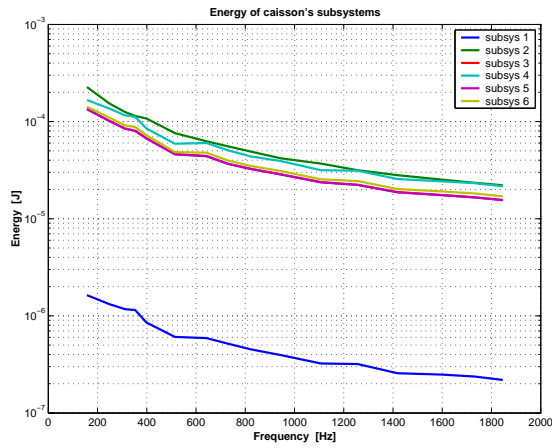
(a) Caisson
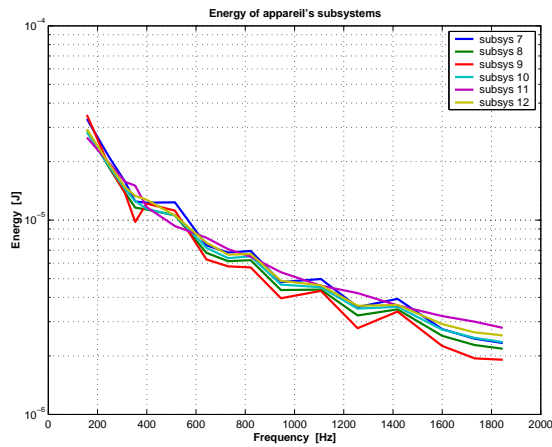
(b) Appareil
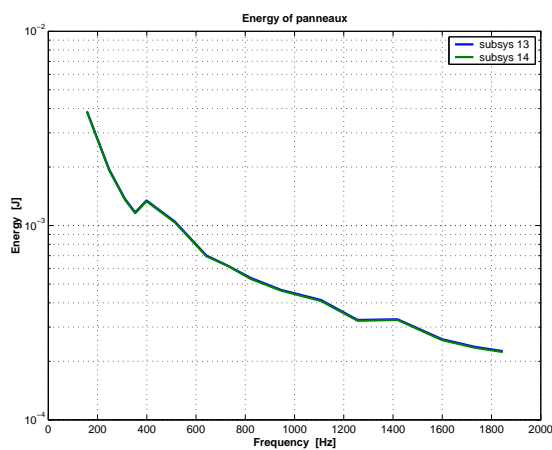
(c) Panneaux

Figure 12: Energies of Nanosat's subsystem
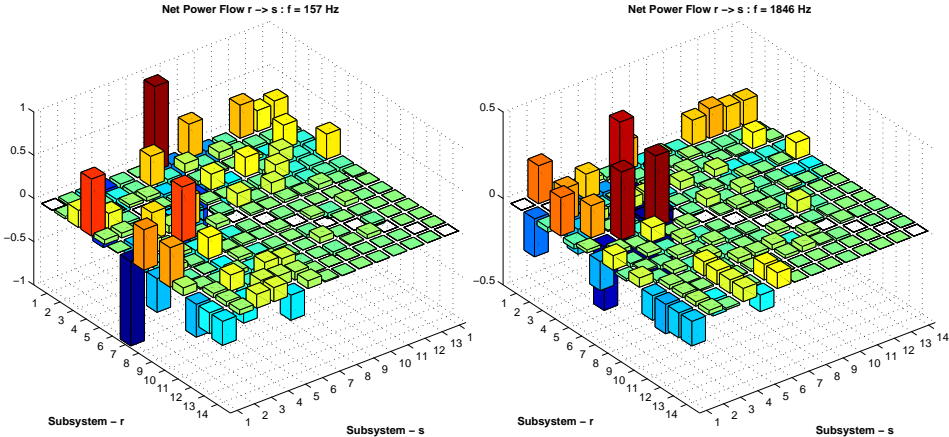
(a) view 3D
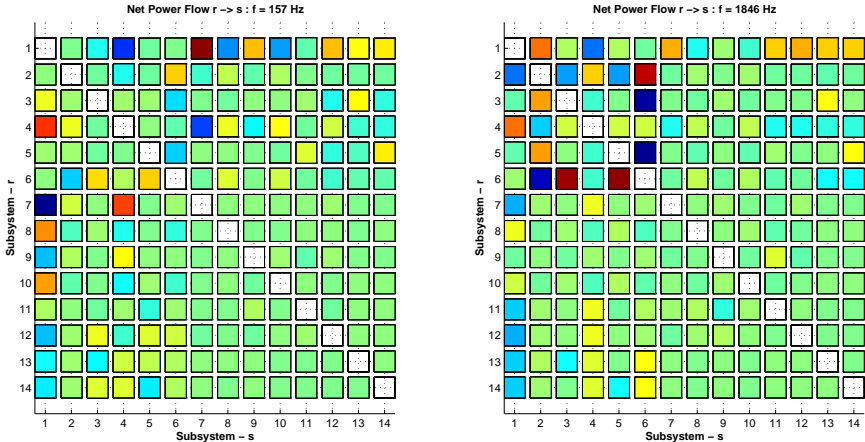
(b) view 2D

Figure 13: Net power flows of Nanosat

4 | ACCELERATION

Probably, the acceleration is the more interesting characteristic for the dynamic analysis. For this reason different methods were developed to obtain it by SEA characteristics (energy and power). This chapter will show these methods and in particular the theory behind them and theirs interest.

4.1 DIRECT ACCELERATION

The first method that was developed is the most easy and immediate. In fact, the acceleration was obtained directly by the energy estimated with the Quasi-SEA method (§ 2.1).

4.1.1 Theory

Starting with the equation of the kinetic energy:

$$T = \frac{1}{2}mv^2 \tag{4.1}$$

Hence, knowing that in the frequency domain the relation between velocity and acceleration is $a = \omega v$. Considering the maximal value of acceleration and replacing the velocity in the previous equation:

$$T_{max} = \frac{1}{2}m\left(\frac{A}{\omega}\right)^2 \tag{4.2}$$

where A is the maximal value of acceleration. By the hypothesis that, for the SEA, the kinetic and potential energy are equal it is possible to write the acceleration in g as:

$$g = \sqrt{\frac{E_{sea}\omega^2}{9.81^2 \cdot m}} \tag{4.3}$$

where E_{sea} is the energy in the band and ω is the center band frequency.

4.1.2 Applications and results

The simple model of the cube was analysed to validate the code. After the choice of the subsystems' points, necessary to solve the Quasi-SEA method, a unitary force was applied to one point of one subsystem to simulate the perturbations of a gyroscope. Then, the velocities for each subsystem were evaluated by the sinus analysis. Knowing the force injected and the velocity, the input power was defined. The physical characteristics of the Quasi-SEA method were evaluated by this input power. For a gyroscope it is possible to obtain the power by the equivalent exiting force and the surface mobility [6]. Thus, the accelerations were calculated with the method illustrated in § 4.1.1. Finally, the accelerations obtained by Quasi-SEA method and sinus analysis were compared. The calculation's sequence is illustrated in Fig. 14 on the next page.

Cube model: 6 subsystems

In Fig. 15 on page 32, the dashed lines represent the acceleration by sinus analysis in different points of the subsystem and the continuous line with a triangular marker represents the acceleration obtained by Quasi-
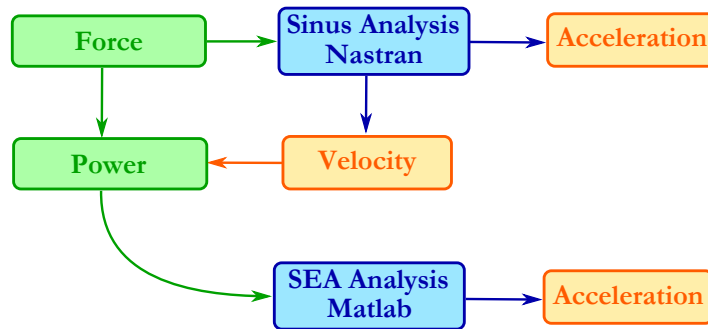
Figure 14: Calculation's sequence for the accelerations

SEA. In general, the value of acceleration obtained by Quasi-SEA is near to the average value of acceleration of the subsystem. In Fig. 15c the acceleration by Quasi-SEA is nearer to the continuous line without marker, which represents the acceleration of the point where the power was injected.

Moreover, a study, with different limit conditions, allowed to observe a connection between the type of block and the acceleration. In particular, three cases were considered: in the first case the third subsystem was joined with the near subsystems (modeled by a merging of the edge's points), while in the last two cases the third subsystem was connected with the near subsystems by four bolts per edge, in one case the rotations of the bolts were allowed and in the other all the DoF were blocked. Comparing the results showed in Fig. 16 on page 33 it is possible to notice that the deviation between the estimated acceleration and the average acceleration of the sinus analysis is bigger when there are more DoF. Additionally, there is not much difference between the SEA's accelerations of the case *(a)* and *(b)* which shows that the SEA is less sensible to little block's changes.

The analysis of the subsystems' energy was started to find an explanation to the particular behavior observed in Fig.16. How it was expected, the same behavior of the acceleration of the 3rd subsystem was found in the energy. Moreover, the total energy of the system is the same for the two analyses (Quasi-SEA and sinus) despite the different value of energy in the subsystems (Fig. 17 on page 34). Thus, it means that there is not energy dissipation but only a different power engineering. It is easy to notice that the energies (and also the accelerations) of the subsystems are similar. They have different values but the same progress. The explanation could be found in the Eq. 2.1, in fact, the energy is estimated by the power injected so, if a subsystem is not stimulated, this subsystem does not participate to the energy's solution. In the studied model, only the

(a) Acceleration 1st subsystem

(b) Acceleration 3rd subsystem

(c) Acceleration 5th subsystem
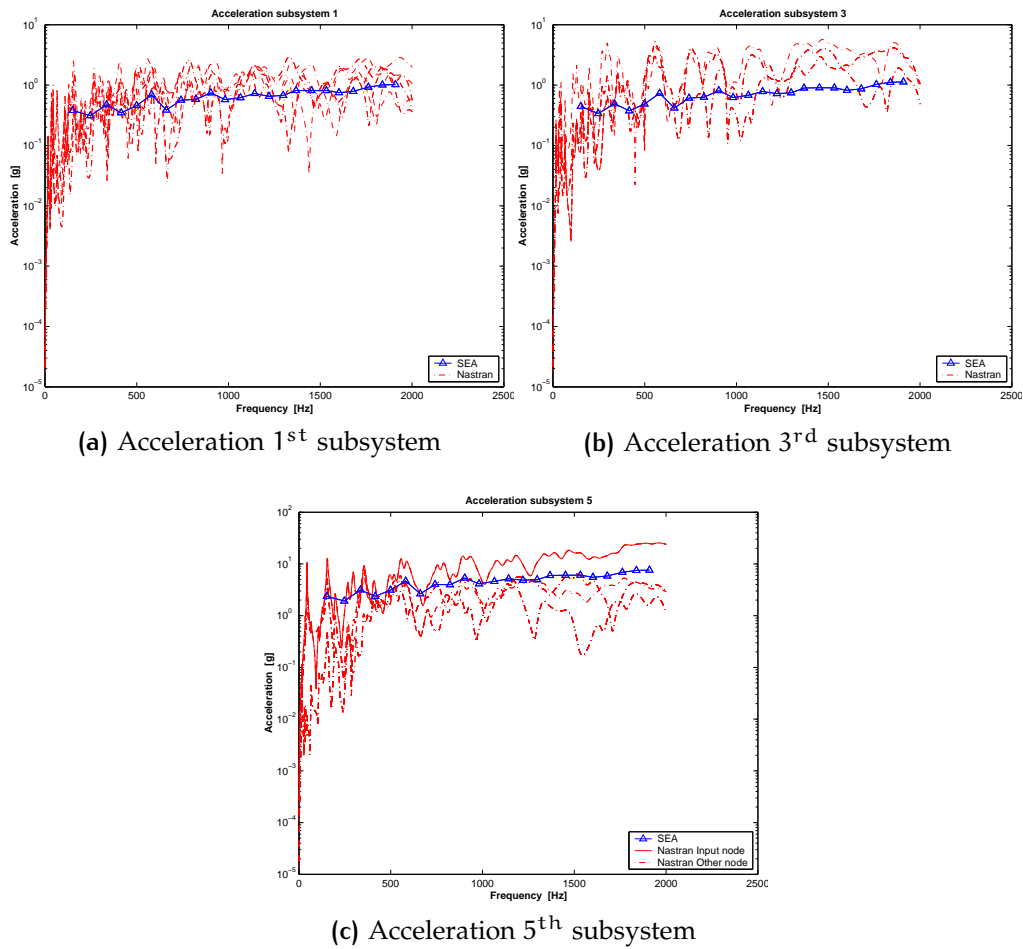
Figure 15: Accelerations, Power in 5th ss. in 1 point – Merged

5th subsystem had an input power, so that, the energy of all subsystems depends only on $P_{in}^{(5)}$.

Observing the energy of the 5th subsystem (Fig. 17c) a well approximation of the Quasi-SEA is immediately seen. Hence, a further analysis with all subsystems stimulated was performed. As researched, the energy obtained by Quasi-SEA is in all subsystems a good interpolation of the energy obtained by the sinus analysis(Fig. 18 on page 35).

The acceleration is directly connected to the energy, so a bad estimation of the latter implies a bad estimation of the acceleration. However, the results show a value of acceleration acceptable despite a value of energy not acceptable. The difference between the energy's values of the Quasi-SEA and the sinus analysis (Fig. 17), despite the results were obtained
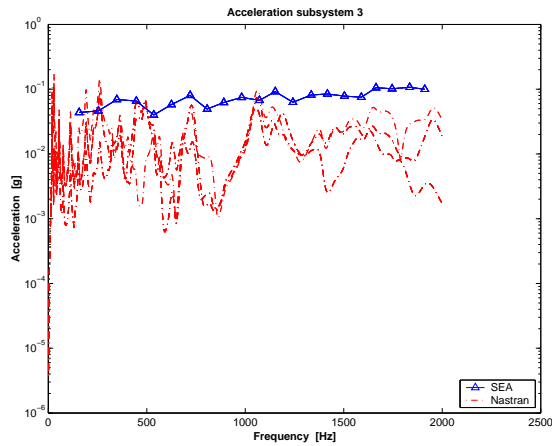
(a) Case DoF $1-3$ blocked
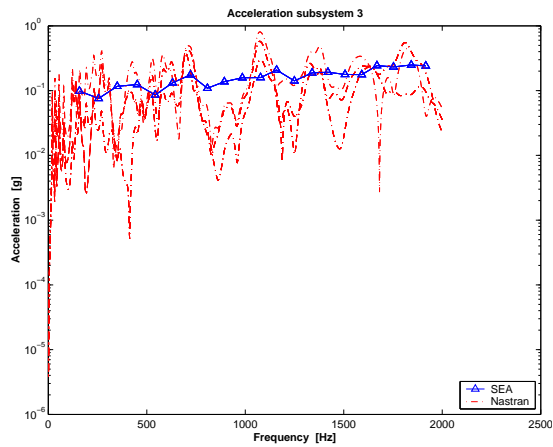
(b) Case DoF $1-6$ blocked
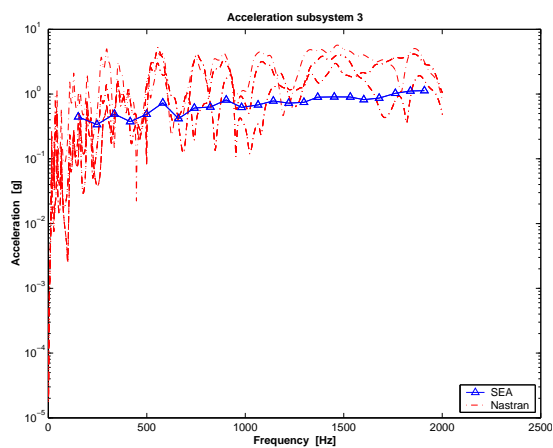
(c) Case merged

Figure 16: Accelerations 3rd ss., Power in 5th ss. in 1 point

(a) Energy 1ˢᵗ subsystem

(b) Energy 3ʳᵈ subsystem

(c) Energy 5ᵗʰ subsystem

(d) Total Energy system
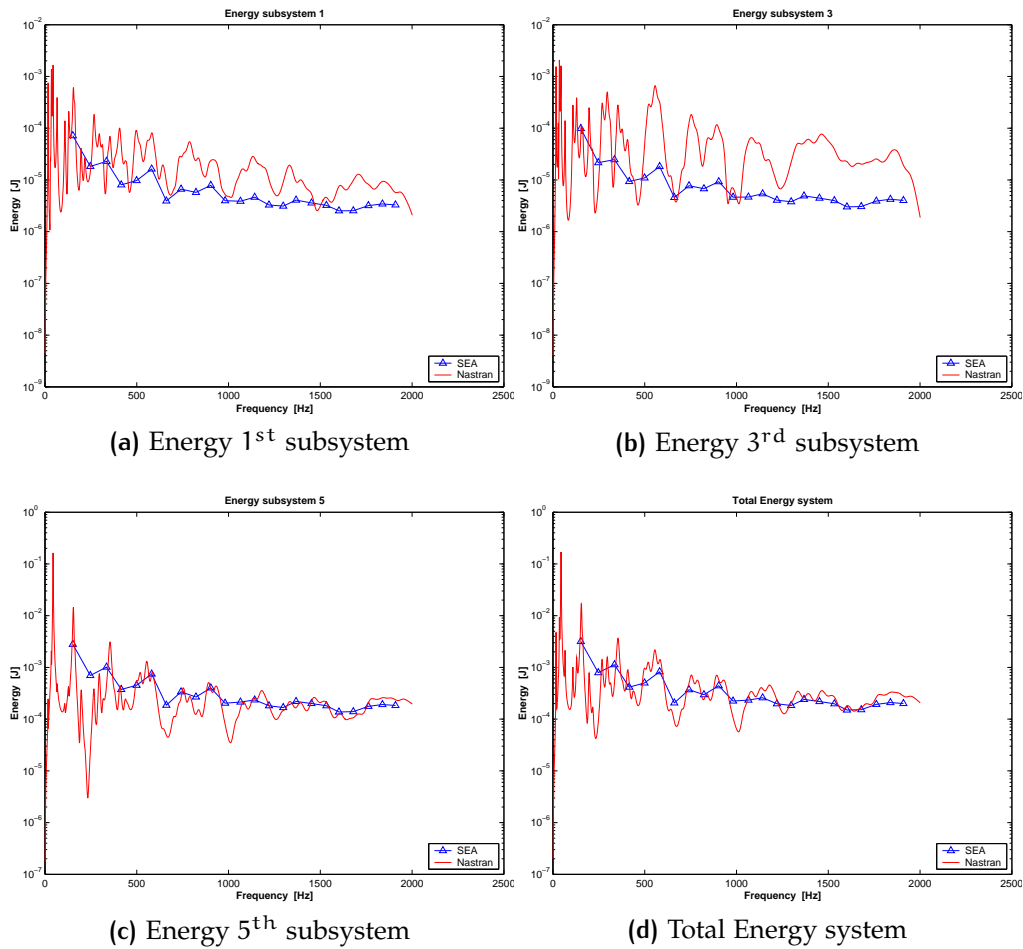
Figure 17: Energies, Power in 5ᵗʰ ss. in 1 point – Merged

by the same base of data (the modal shape given by Nastran), could be explained by the resolution's method of Eq. 2.1 as discussed on page 31.

Analysing the results of the energies for the two cases (one or all subsystems stimulated), it is possible to note that an error of estimation is always present for frequencies smaller than 400 Hz, in particular for the total energy and the subsystem stimulated. In fact, the SEA does not guarantee a good solution for frequencies smaller than $400 - 500$ Hz [16, 17]. Different methods were developed to apply the SEA in this range of frequency. But, the results could be accepted because they are overestimated.

(a) Energy 1st subsystem

(b) Energy 3rd subsystem

(c) Energy 5th subsystem

(d) Total Energy system
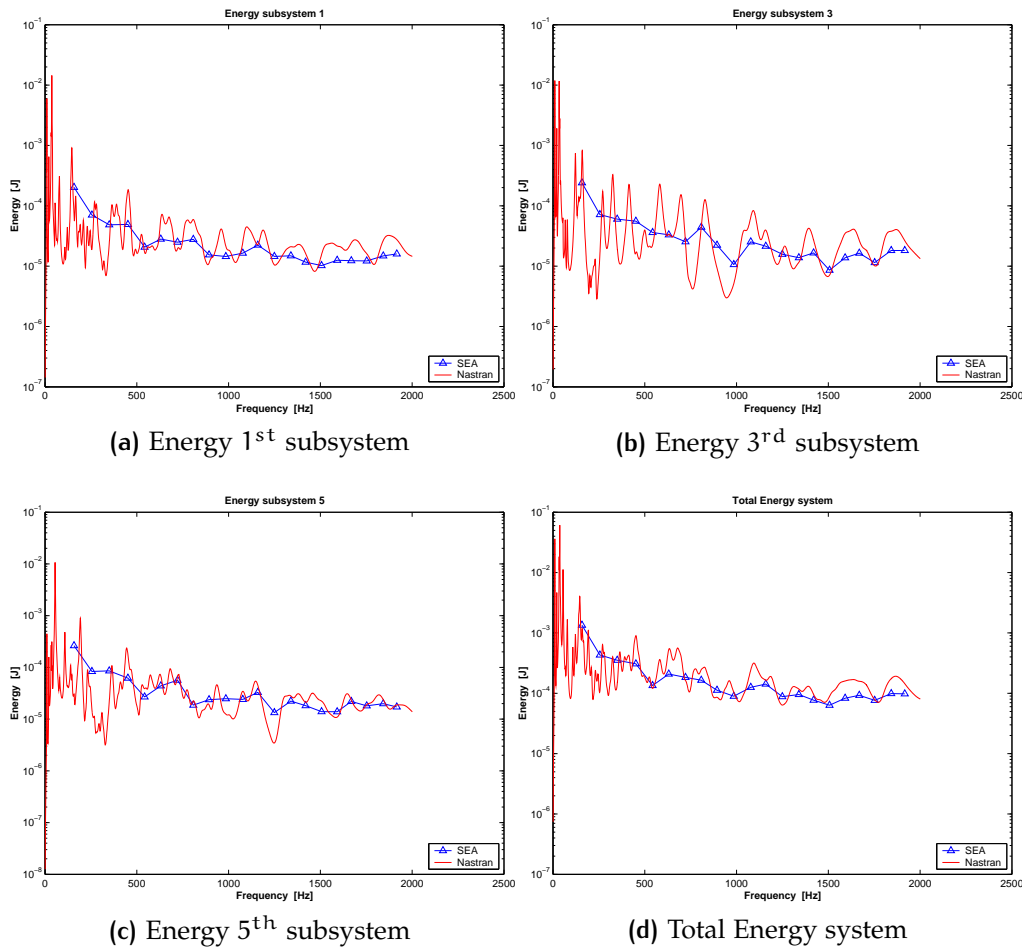
Figure 18: Energies, Power in *All* ss. in 1 point – DoF 1-6 blocked

Cube model: 7 subsystems

Because the SEA is based on the choice of the system's decomposition, a different division in subsystems was analysed. In particular, a seventh subsystem composed by one point was added in the fifth and the power was injected in this seventh subsystem. These variations implied a remarkable changing in the final results, as showed in Fig. 19 on the following page, confirming the importance of the choice of the subsystems for the resolution with the SEA method. As expected, the accelerations of the 7th subsystem coincide (Fig. 20) and the acceleration of the 5th subsystem, which was obtained with the Quasi-SEA, does not change. In fact, considering the position of the 5th subsystem compared with the 3rd it is possible to say that the 5th is directly exited. Nevertheless, the other
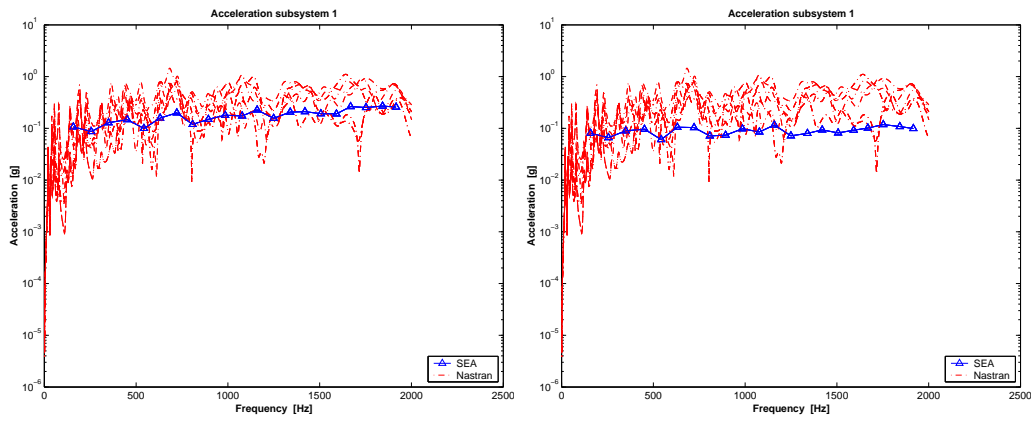
(a) Acceleration 1st subsystem
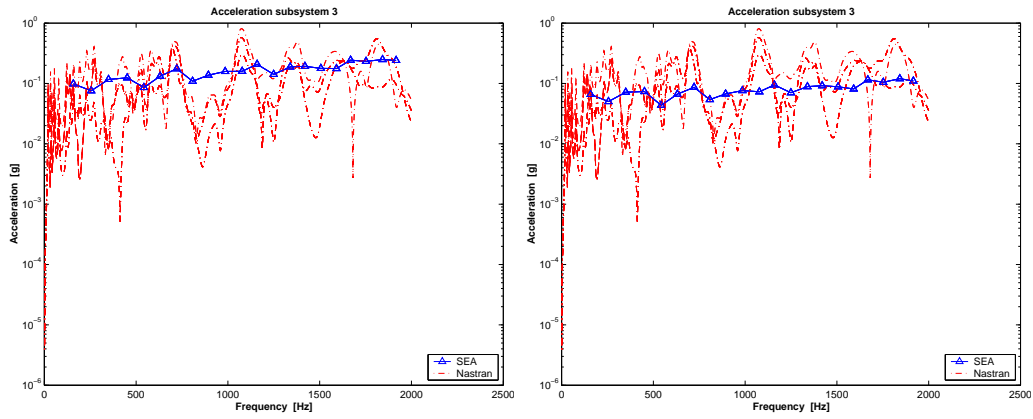
(b) Acceleration 3rd subsystem
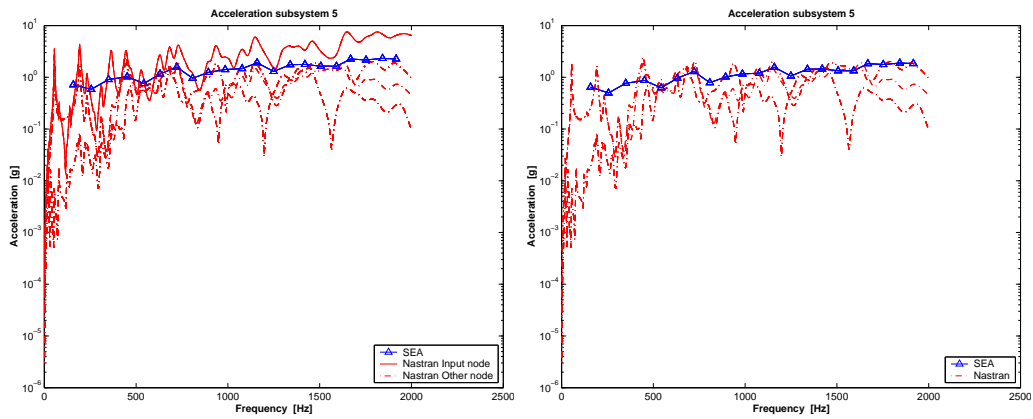
(c) Acceleration 5th subsystem

Figure 19: Acceleration, DoF 1-6 blocked, **left**: Cube 6 ss., **right**: Cube 7 ss.
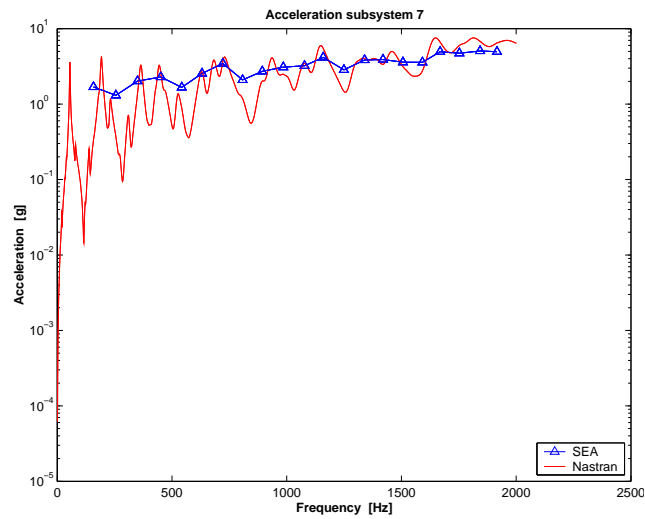
(a) Acceleration

Figure 20: Acceleration 7th subsystem, DoF 1-6 blocked

subsystems show an evident decreasing of the accelerations relative to the case with six subsystems (Fig. 19 left).

Despite if there are many rules to choose the subsystems, the choice always depends on the user. A method of automatic substructuring that does not consider the "human effect", and that yield interesting results, was suggested by Gagliardini et al. [8]. It is important to say that this method does not satisfy the requests of the SEA which works with a homogeneous subsystem [1, 6]. The division of a system is still a field of research.

4.1.3 Considerations

The *direct acceleretion* method is interesting because it removes the problem of the evaluation of equivalent masses. Moreover, the necessary solving time is short, so, it could be used to know quickly the average value of the acceleration.

4.2 ACCELERATION BY MOBILITY

The second method burns by the desire of a better estimation of the acceleration starting by the relation between the subsystems. In different reports and articles, the estimation of the acceleration starts by the evalu-

ation of the mobility and the equivalent mass. In particular, to estimate the equivalent mass is very difficult, in addition, it is an artificial value and it has no physical proprieties. For these reasons, and in particular for the last two, a new method was suggested and developed.

4.2.1 Theoretical base

Considering a system divided in n_s subsystem that respects the SEA hypothesis. Each subsystem is excited by random, stationary, and distributed forces. It is assumed that the system is linear and that the excitations which are applied to the different subsystems are uncorrelated.

The power W_r of a subsystem r could be expressed as:

$$W_r = \langle F_r \rangle \cdot \langle v_r \rangle \tag{4.4}$$

where $\langle F_r \rangle$ is the mean force acting on the subsystem r, and $\langle v_r \rangle$ the mean vibration velocity. The latter depends on forces which act on each subsystem by mobility $\langle v_r^2 \rangle = |Y|^2 \langle F^2 \rangle$. Thus, the velocity generated on the subsystem r by a force F_s in the subsystem s will be equal to $\langle v_{rs}^2 \rangle = |Y_{rs}|^2 \langle F_s^2 \rangle$. Considering a frequency band Ω, we can express the power of the subsystem 1 as:

$$
\begin{aligned}
W_{1,\Omega} &= \langle F_1 \rangle_\Omega \cdot \langle v_1 \rangle_\Omega \\
&= \langle F_1 \rangle_\Omega \sum_{r=1}^{n_s} \langle v_{1r} \rangle_\Omega \\
&= \langle F_1 \rangle_\Omega \sum_{r=1}^{n_s} \left[|Y_{1r}|_\Omega \cdot \langle F_r \rangle_\Omega \right]
\end{aligned}
\tag{4.5}
$$

Re-writing this equation for each subsystem:

$$
\left\{ \begin{array}{c} W_1 \\ \vdots \\ W_{n_s} \end{array} \right\} = \left[\begin{array}{ccc} Y_{11}F_1 & \cdots & Y_{1n_s}F_1 \\ \vdots & \ddots & \vdots \\ Y_{n_s1}F_{n_s} & \cdots & Y_{n_sn_s}F_{n_s} \end{array} \right] \left\{ \begin{array}{c} F_1 \\ \vdots \\ F_{n_s} \end{array} \right\}
\tag{4.6}
$$

$$\{W\} = [Y(F)]\{F\} \tag{4.7}$$

The mobility matrix $\mathbf{Y}$ is known, it is evaluated by FRF or sinus analysis. Moreover, knowing that the power is connected to the energy by $W_r =$

$\omega \langle E_r \rangle$, where the energy $\langle E_r \rangle$ is obtained by SEA analysis, it is possible to solve the nonlinear system (4.7) to obtain the velocity and acceleration for each subsystem

$$\langle v_r \rangle = \sum_{s=1}^{n_s} Y_{rs} \langle F_s \rangle$$
$$\langle a_r \rangle = \omega \langle v_r \rangle$$

(4.8)

where ω is the center band frequency of Ω.

4.2.2 Applications and results

The same calculation's sequence used for the analysis of the *direct acceleration* (§ 4.1.2) was used for the *acceleration by mobility*. Because this second method starts by the hypothesis in eq. 4.4, it is necessary to have an input power in the subsystem to estimate the acceleration. Then, the case where each subsystem is stimulated by an input power is the only case which was analysed.

It is possible to catch the likeness of the results between the accelerations obtained by Nastran and this second method. It is important to point out that in the SEA method all the subsystems are stimulated by the input power. Consequently, it is clear that the acceleration is similar to the acceleration of the point where the force is injected (Fig. 21 on the next page).

4.2.3 Considerations

This result shows the effectiveness of the method illustrated in § 4.2.1. This method is interesting because, as the first method, it removes the problem of the evaluation of equivalent masses. Moreover, it obtains an acceleration near the maximal acceleration of the subsystem.

The limit of this second method is that it could not be applied if not all subsystems are stimulated. Thus, it is efficient for a vibroacoustic analysis. Another limit is the solving time; in fact this method is extremely slow. For example, in the case of the model which was analysed a time of 20 min is necessary to obtain the results, whereas only few seconds are necessary with the first method. However, the solving time could be reduced if the mobility matrix will be memorised, who does not change with the charge conditions but only with the geometry. Then, a change in the load condition will not imply a repetition of the calculations.
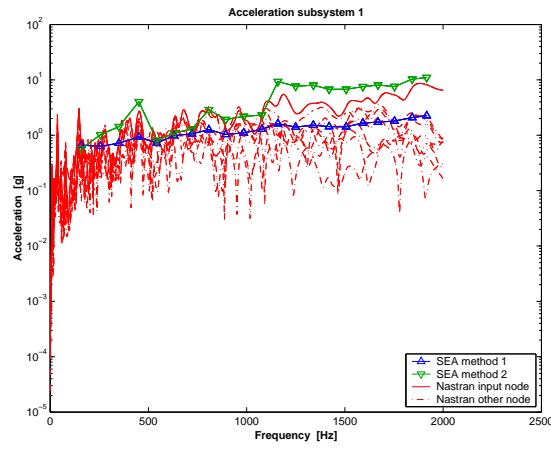
(a) Acceleration 1st subsystem, Methods 1 and 2
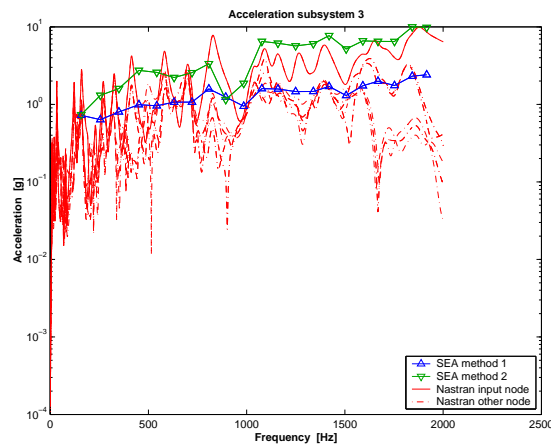
(b) Acceleration 3rd subsystem, Methods 1 and 2
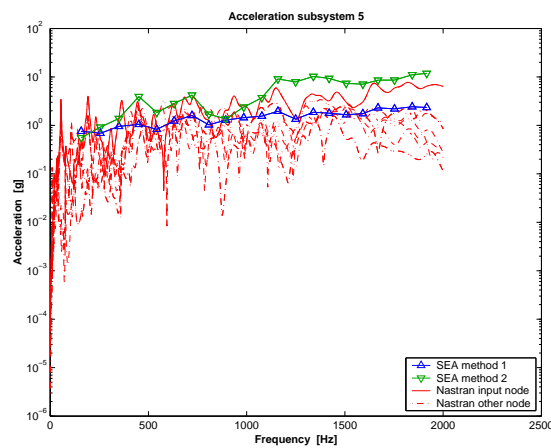
(c) Acceleration 5th subsystem, Methods 1 and 2

Figure 21: Accelerations, Power in *All* ss. in 1 point – DoF 1-6 blocked

4.3   ACCELERATION BY α_j

The third method was developed to understand the hypothesis behind the SEA analysis. In fact, it is not clear how the energy of the band is allocated between the modes. The SEA considers energy's distribution proportional to the mode's contribution, and then the mode with a bigger response receives a bigger quantity of energy, or an uniform distribution between the modes. The most argued idea was how the energy of the band was allocated in a uniform way and the results had confirmed this hypothesis.

4.3.1   Theory

Starting by equation of the kinetic energy:

$$T = \frac{1}{2}\dot{q}^T M \dot{q} \tag{4.9}$$

where $\dot{q}$ is the velocity and M is the mass matrix. For a point of the structure, the following relation between the velocity and the modal shapes is hold:

$$\dot{q}_n = \sum_j \alpha_j \omega_j \phi_j(x_n) \tag{4.10}$$

Then, the kinetic energy of the system could be written as

$$\begin{aligned}
T &= \frac{1}{2}\dot{q}^T M \dot{q} \\
&= \frac{1}{2}\Big(\sum_j \alpha_j \omega_j \phi_j\Big)^T M \Big(\sum_k \alpha_k \omega_k \phi_k\Big)
\end{aligned} \tag{4.11}$$

Finally, the kinetic energy of a subsystem r attributable to the mode j is defined as

$$T_j^{(r)} = \frac{1}{2}\sum_{n \in r}\left[\big(\alpha_j \omega_j \phi_j(x_n)\big)^T M_n \big(\alpha_j \omega_j \phi_j(x_n)\big)\right] \tag{4.12}$$

Where α_j is the only unknown parameter. In fact, the natural frequencies and modal shapes are obtained by Nastran and the kinetic energy $T_j^{(r)}$ is obtained by Quasi-SEA analysis, $E^{(r)} = 2T^{(r)}$ (see § 2.1.2). Hence, the

acceleration $\ddot{q}_n$ of a point n is quickly defined knowing the parameters α_j

$$\ddot{q}_n = \sum_j \alpha_j \omega_j^2 \phi_j(x_n) \tag{4.13}$$

and so, the acceleration of a whole subsystem

$$\ddot{q}^{(r)} = \frac{1}{N_p^{(r)}} \sum_n^{N_p^{(r)}} \ddot{q}_n \tag{4.14}$$

However, the calculated acceleration present errors, so correction is needed. In fact, starting by the kinetic energy of a subsystem (e.g. r) and by the hypothesis of a uniform energy's distribution between the modes, it is possible to write:

$$T^{(r)} = N_m \cdot T_j^{(r)} \tag{4.15}$$

where N_m is the number of modes in the frequency band. By Eq. 4.17 the kinetic energy becomes:

$$T^{(r)} = \frac{1}{2} M^{(r)} \frac{N_m}{N_p^{(r)}} \sum_n \left(\alpha_j^2 \omega_j^2 \phi_j^2(x_n) \right) \tag{4.16}$$

The part $\sum_n \left[\alpha_j^2 \omega_j^2 \phi_j^2(x_n) \right] = \beta$ is constant by the hypothesis of uniform energy's distribution, hence:

$$T^{(r)} = \frac{1}{2} M^{(r)} \frac{N_m}{N_p^{(r)}} \beta \tag{4.17}$$

Starting by the equation of the acceleration (Eq. 4.14) and replacing $\ddot{q}_n$ with the Eq. 4.13, the following development is worth

$$\begin{aligned}
\tilde{a}^2 &= \frac{1}{N_p^{(r)2}} \left[\sum_n \ddot{q}_n^2 + \sum_n \sum_{t \neq n} \ddot{q}_n \ddot{q}_t \right] \\
&= \frac{1}{N_p^{(r)2}} \left\{ \beta \left[\left(N_m \omega \right)^2 - \sum_j \sum_{k \neq j} \omega_j \omega_k \right] + \right. \\
&\quad \left. + \sum_j \sum_{k \neq j} \left[\omega_j \omega_k \sum_n \left(\alpha_j \omega_j \phi_j(x_n) \cdot \alpha_k \omega_k \phi_k(x_n) \right) \right] \right\}
\end{aligned} \tag{4.18}$$

In the simple case of a subsystem constituted by only one point, the previous equation becomes

$$\tilde{a}^2 = \beta \left(N_m \omega \right)^2 \tag{4.19}$$

Then, replacing this equation in the Eq. 4.17 and comparing it with Eq. 4.2

$$\begin{cases} T^{(r)} = \frac{1}{2} M^{(r)} \frac{N_m}{N_p^{(r)}} \beta = \frac{1}{2} M^{(r)} \frac{1}{N_m} \left(\frac{\tilde{a}}{\omega} \right)^2 \\ T^{(r)} = \frac{1}{2} M^{(r)} \left(\frac{a}{\omega} \right)^2 \end{cases} \tag{4.20}$$

it is possible to obtain the relation between the two types of acceleration

$$\tilde{a} = a \sqrt{N_m} \tag{4.21}$$

That means that the calculated acceleration with the third method is bigger than the acceleration obtained with the first method. This result is valid only for a subsystem of one point and under the hypothesis of uniform energy distribution. In the case of a subsystem composed by different points a simplification of the Eq. 4.18 is more difficult but, it is possible to use the Cauchy-Schwarz inequality to obtain a sign condition. The sum of the latter two terms in the equation is always negative then, it could be written:

$$\tilde{a}^2 \geqslant \beta \left(\frac{N_m \omega}{N_p^{(r)}} \right)^2 \tag{4.22}$$

Hence, comparing the two forms of the subsystem's energy as in the previous case:

$$\tilde{a} \sqrt{\frac{N_p}{N_m}} \geqslant a \qquad \qquad \tilde{a} \geqslant a \sqrt{\frac{N_m}{N_p}} \tag{4.23}$$

4.3.2 Validation of theory

The same cube model used for the first and second method was analysed. However, a different decomposition in subsystems was necessary to verify the hypothesis and the expected results depicted in the previous paragraph. In that case eight subsystems were chosen; in particular the
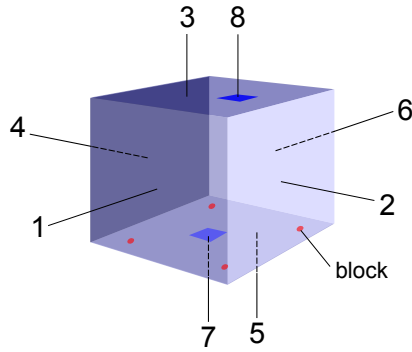
Figure 22: cube model, 8 subsystems

7th subsystem was constituted by only *one point* (to confirm Eq. 4.21) and it was localized in the center of the 5th subsystem. Moreover, the input power was injected in the 7th subsystem. The 8th subsystem is constituted by *two points* and it was localized in a off-center position in the 3rd subsystem. This subsystem was generated to represent an observing point. A global view of the model was represented in Fig. 22.

In Figures 23 and 24 the accelerations obtained by the first and third method were compared. The acceleration of the third method was corrected with the factor $\sqrt{\frac{N_p}{N_m}}$ and it is possible to observe the coincidence with the results in the 7th subsystem (Fig. 24a), as predicted by the Eq. 4.21. Whereas in the other subsystems who consist of more points, the acceleration obtained by the third method is always bigger than the first as explained in Eq. 4.23.

4.3.3 Peculiarities of the third method

With this third method is possible to concentrate the energy in a mode, then, it is possible to find the mode that generates the maximal and minimal average acceleration in the subsystem. These two accelerations were plotted in the graph by a green band and unlike the expected results, these two values did not gave any additional information.

An easy and quick method to evaluate the last terms of the Eq. 4.18, the value of overestimation, is to apply and compare, sequentially, the first and third method (*direct acceleration* and *acceleration by* α_j).

$$\gamma = \frac{a(\omega)|_{1^{\text{st}}\text{method}}}{a(\omega)|_{3^{\text{rd}}\text{method}}} \tag{4.24}$$
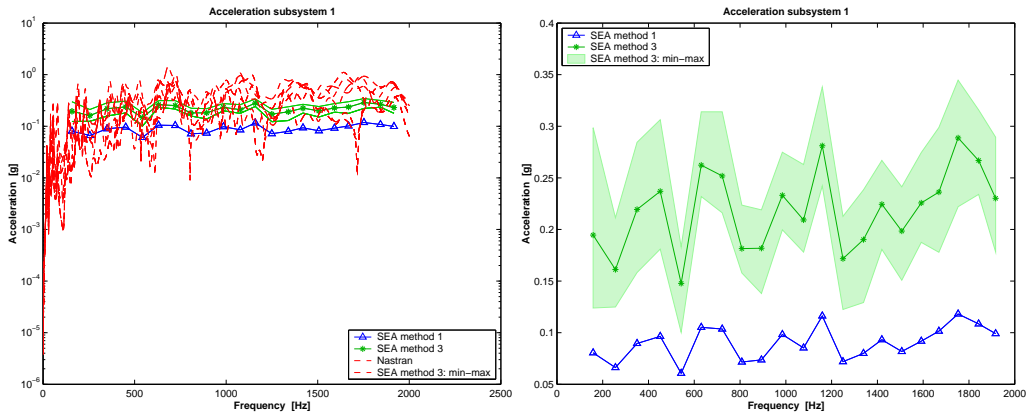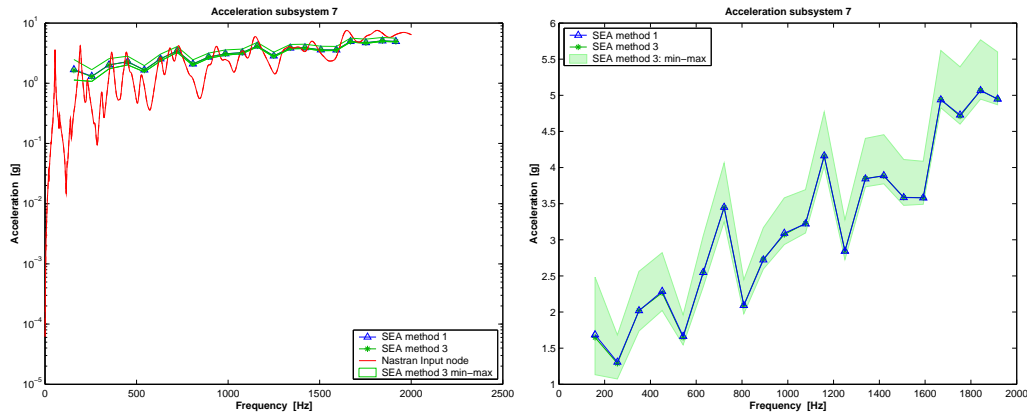
(a) Acceleration 1st subsystem,
Methods 1 and 3
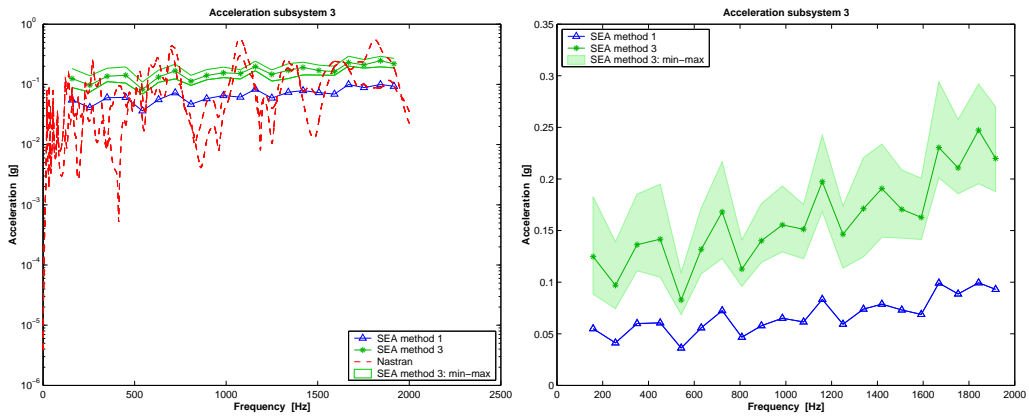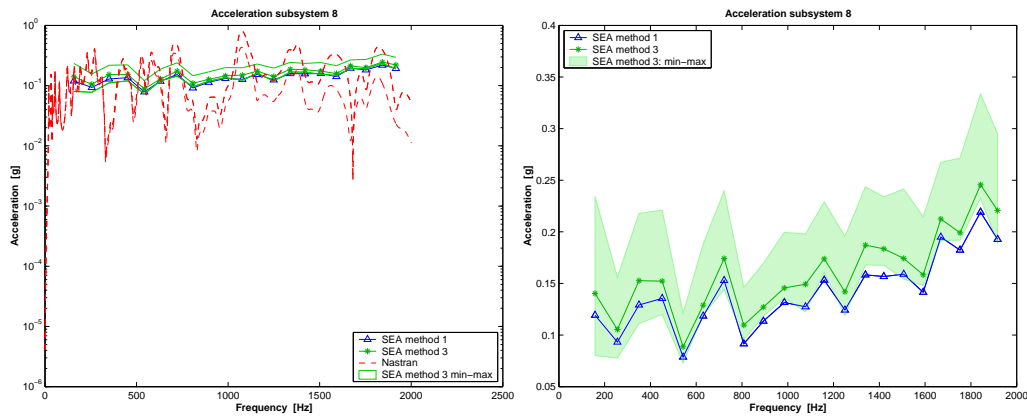

(b) Acceleration 3rd subsystem,
Methods 1 and 3
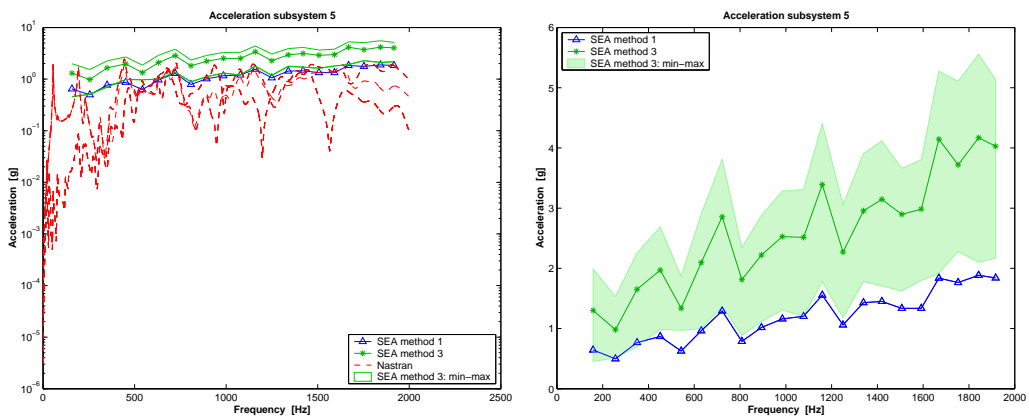
(c) Acceleration 5th subsystem,
Methods 1 and 3

Figure 23: Accelerations, Power in 7th ss. – DoF 1-6 blocked

(a) Acceleration 7th subsystem,
Methods 1 and 3

(b) Acceleration 8th subsystem,
Methods 1 and 3

Figure 24: Accelerations, Power in 7th ss. – DoF 1-6 blocked

In the first approximation, the γ coefficient is constant. Nevertheless, it is connected to the natural frequencies of the band (ω_j) and the vector shapes ($\phi_j(x_n)$), then, it is not constant in all bands but it changes. After the calculation of γ it will be possible to adjust all the estimations of acceleration obtained by the α_j. In fact, an advantage of this third method is the possibility to estimate the acceleration of a single point as well as the whole subsystem.

It is important an deeper examination about the evaluation of the acceleration in a point. In fact, the acceleration obtained by α_j is the average value in the frequency band who respects the SEA hypothesis, but that is not necessarily the correct value, as showed by the results in Fig. 25 on page 48. Nevertheless, the values could be interpretated as an estimation

of the general behaviour of the point, then, as an indication of a more or less important excitation in the frequency band. Furthermore, comparing the acceleration of two points obtained by Nastran end the SEA an incongruity appears. A more stimulated point (bigger acceleration) for Nastran does not check the results of the SEA, where the same point could be the less stimulated (smaller acceleration). This confirms that was just exposed, the acceleration of a point must be analysed separately by the other and it shows an average behaviour in the bands.

### 4.3.4 A new observed subsystem

In the previous case the 8th subsystem was composed by two points, so for a best generalisation a new 8th subsystem composed only by one point was considered. The results have not shown a change in the solution of the subsystems except in the 8th where the acceleration obtained by the SEA is completely different from the acceleration of Nastran. Comparing the results of the two models (Fig. 25e and 26 on the next pages) it is possible to affirm that a subsystem composed by more points (at least two) is necessary to obtain a result near to the expected result. A different conclusion concern to the stimulated point that could be analysed apart (Fig. 25d).

4.3.5 Selective distribution

A Selective Distribution (SD) was considered to evaluate better the participation of each mode, because the hypothesis of Uniform Energy Distribution (UED) has brought to results not very interesting for the accelerations of the points. In particular, the energy calculated by the SEA was concentrated in a mode then, the acceleration of each point was calculated.

In Fig. 27 on page 50 the acceleration of only one point was plotted (light blue with circle marker); it is possible to observe that if a subsystem is composed by more points the acceleration calculated is not "homogeneous". This sparse result is not observed in the subsystem composed by one point (7th and 8th subsystem) because there is not the coupling between the points described in the acceleration resolution (Eq. 4.17).

For a easier reading, two particular cases was considered: the mean (green Fig. 28 on page 51) and maximal (magenta Fig. 29 on page 52) value of acceleration of each point in the frequency band. Comparing the average accelerations obtained with the acceleration calculated with the
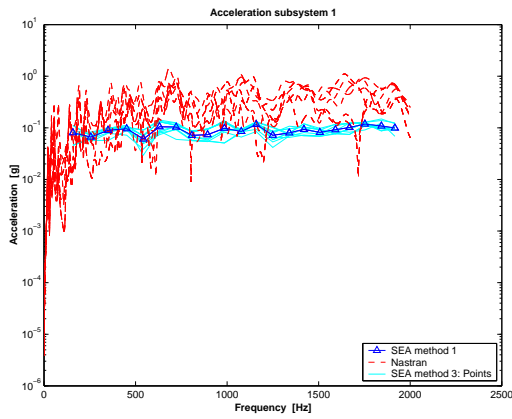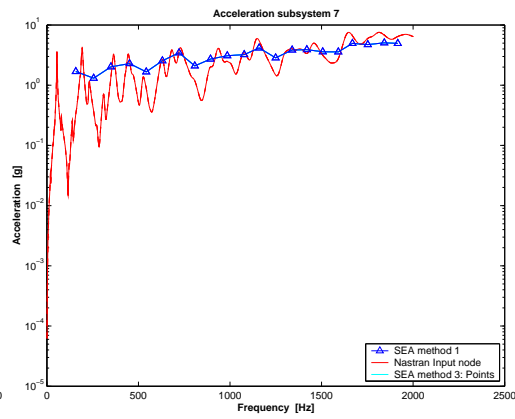
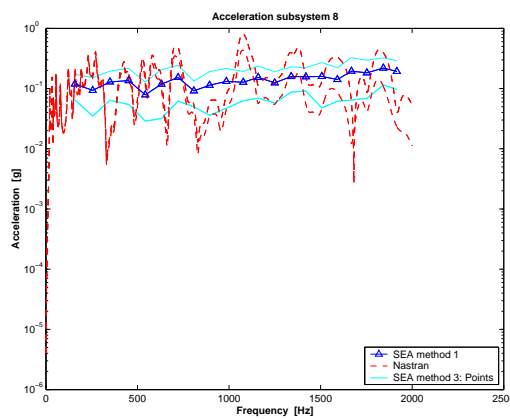**(a)** Acceleration 1st subsystem, Methods 1 and 3
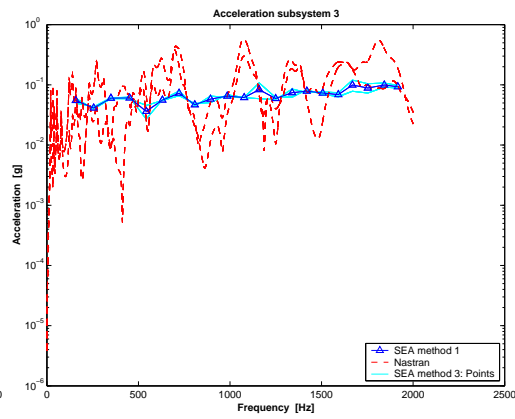
(b) Acceleration 3rd subsystem, Methods 1 and 3
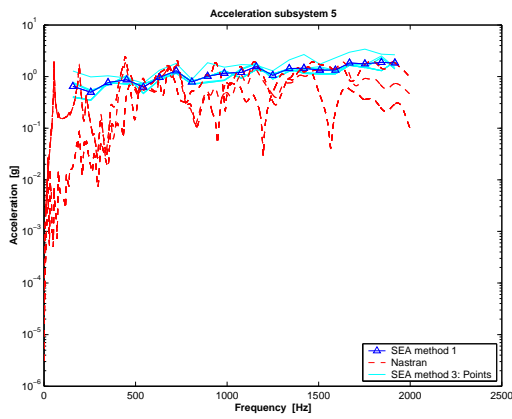
(c) Acceleration 5th subsystem, Methods 1 and 3

(d) Acceleration 7th subsystem, Methods 1 and 3

(e) Acceleration 8th subsystem, Methods 1 and 3

Figure 25: Accelerations, Power in 7th ss. in 1 point – DoF 1-6 blocked
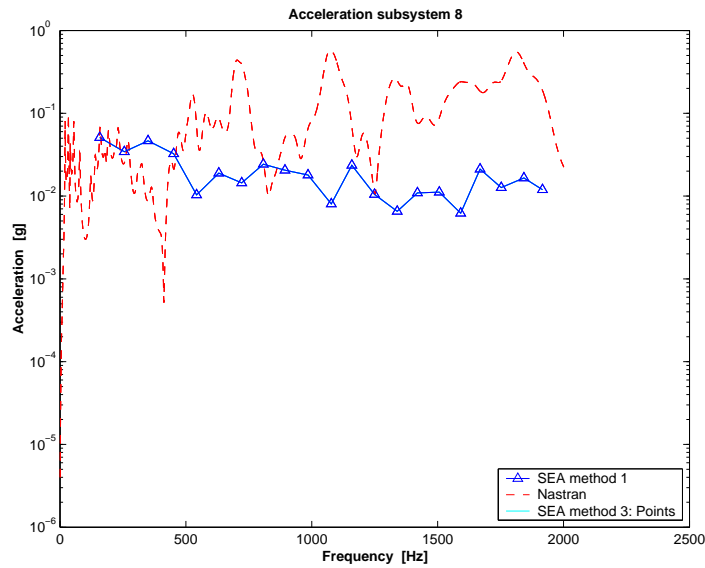
Figure 26: Acceleration 8th subsystem (*one point*), Methods 1 and 3, UED

hypothesis of UED, a clear similarity could be catch. As was expected, the maximal accelerations are localized in a higher range. The acceleration of the 8th subsystem is anyway wrong because the subsystem does not respect the conditions explained in the previous paragraph.

Later on, the average value of the accelerations calculated was considered as interesting results (Fig. 30 on page 53). The average value of the mean accelerations (green with star marker) is near the value of acceleration obtained with the first method (blue with triangular marker), a result that could be expected because the lattes is an average value in frequency and space. However, these two values must coincide so, it is necessary a correction for the acceleration obtained with a UED. Whereas, the average of the maximal acceleration (magenta with square marker) is nearest to the expected values. The 5th subsystem is an interesting case, here the acceleration is near to the acceleration of the stimulated point; in fact, the 7th subsystem is an internal point of the 5th.

The same analysis was applied to the case where all subsystems are stimulated and the results are particularly interesting as observable in Fig. 31, these results could be compared with Fig. 21 on page 40.

4.3.6 Considerations

With this third method is possible to see that each mode participates in an equal way in the resolution of the sea. Moreover, it is possible to
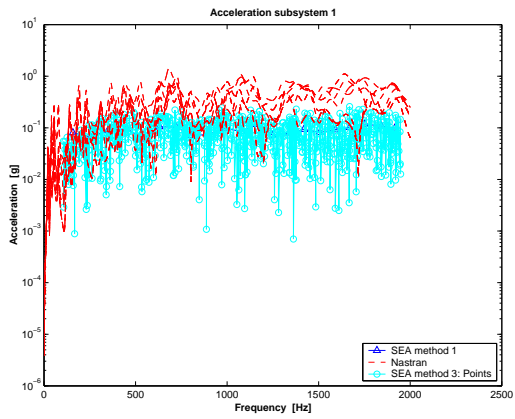
(a) Acceleration 1st subsystem, Methods 1 and 3
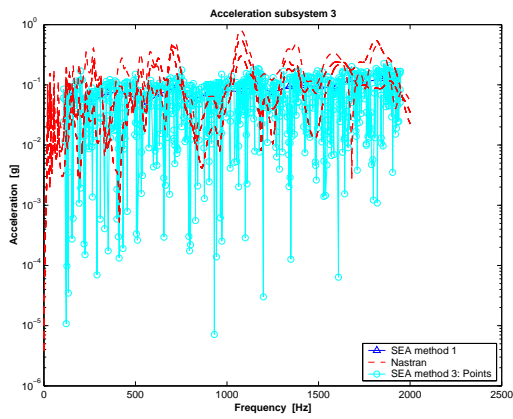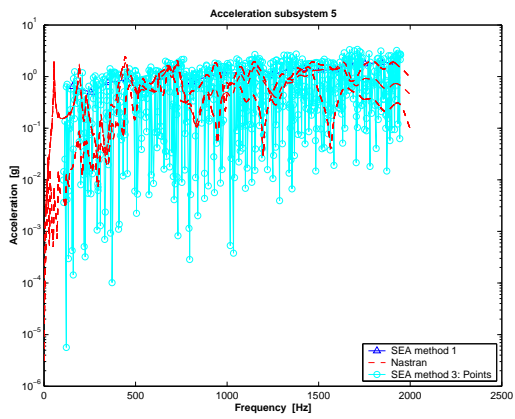
(b) Acceleration 3rd subsystem, Methods 1 and 3

(c) Acceleration 5th subsystem, Methods 1 and 3

(d) Acceleration 7th subsystem, Methods 1 and 3

(e) Acceleration 8th subsystem, Methods 1 and 3

Figure 27: Accelerations, SD

(a) Acceleration 1st subsystem, Methods 1 and 3

(b) Acceleration 3rd subsystem, Methods 1 and 3

(c) Acceleration 5th subsystem, Methods 1 and 3
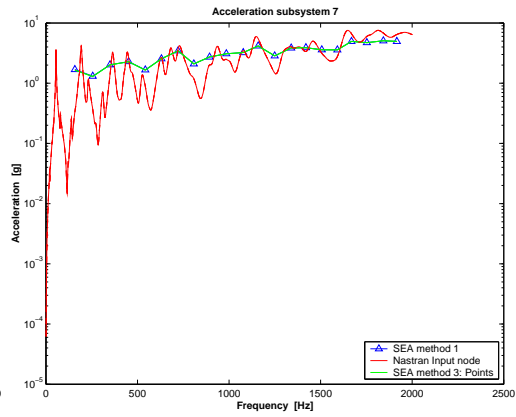
(d) Acceleration 7th subsystem, Methods 1 and 3
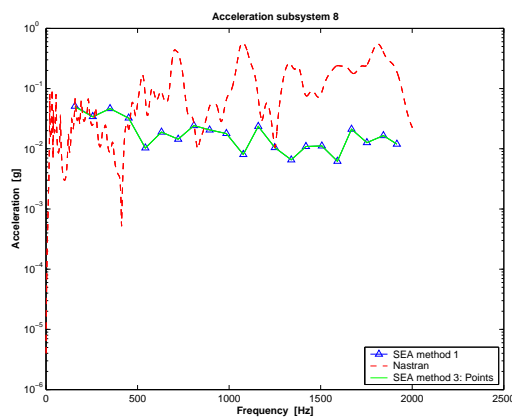
(e) Acceleration 8th subsystem, Methods 1 and 3

Figure 28: Accelerations, SD Average
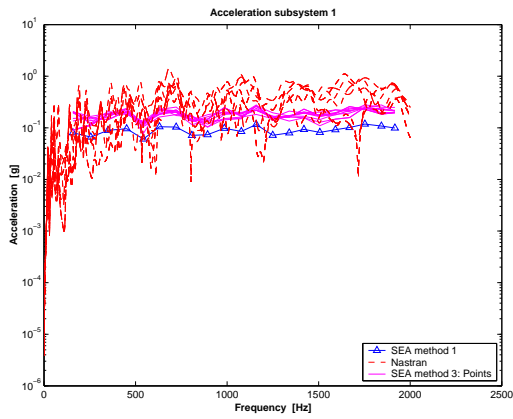
(a) Acceleration 1st subsystem, Methods 1 and 3
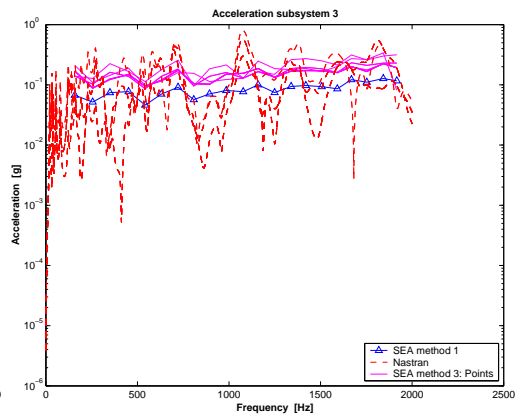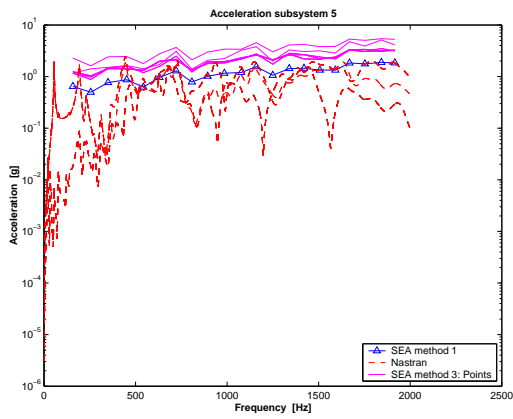
(b) Acceleration 3rd subsystem, Methods 1 and 3

(c) Acceleration 5th subsystem, Methods 1 and 3
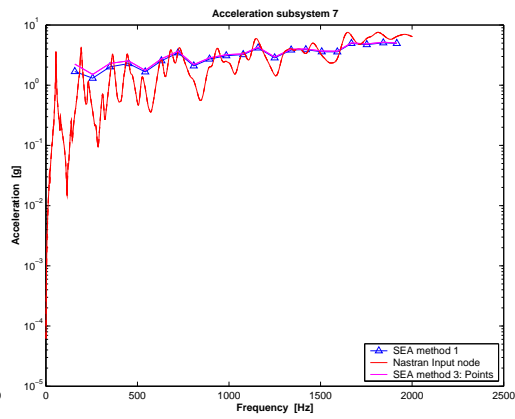
(d) Acceleration 7th subsystem, Methods 1 and 3
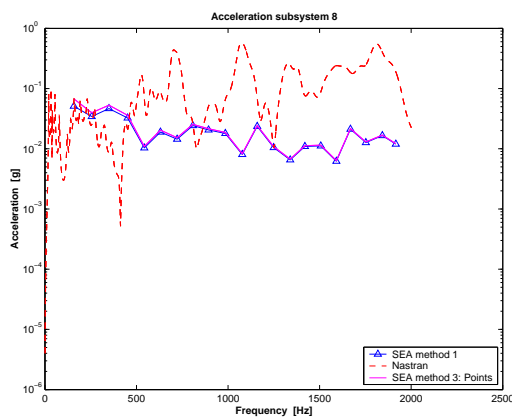
(e) Acceleration 8th subsystem, Methods 1 and 3

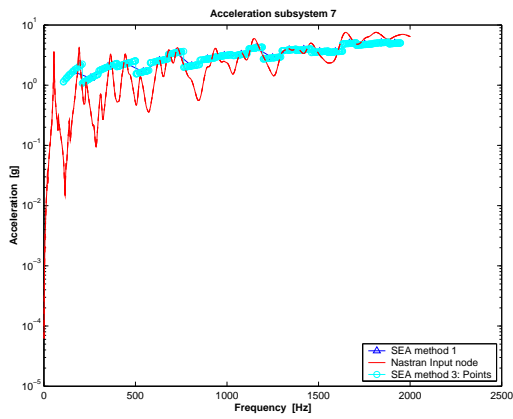**Figure 29:** Accelerations, SD Maximal
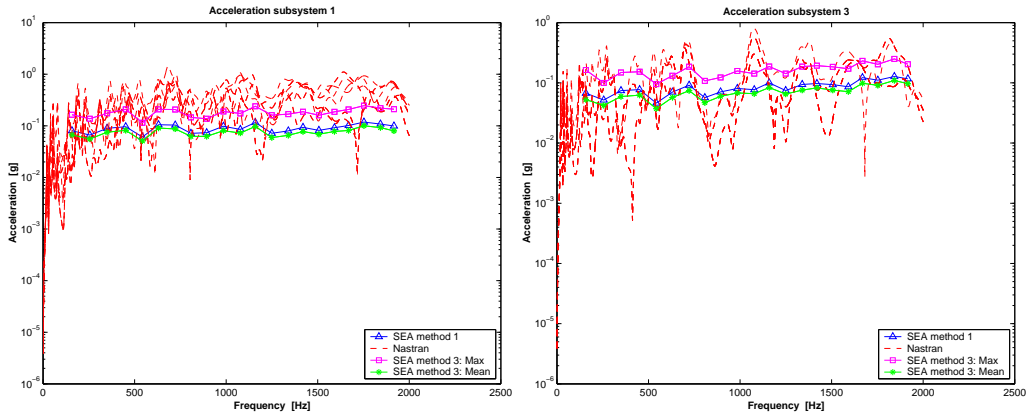
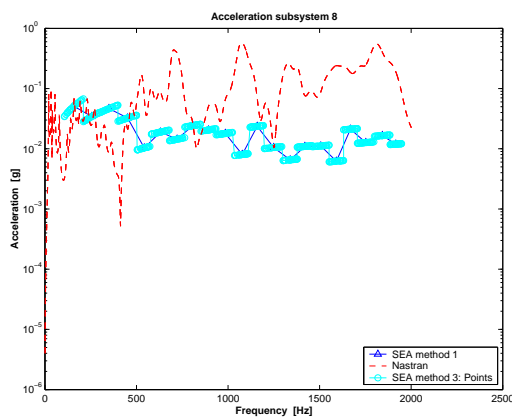(a) Acceleration 1st subsystem, Methods 1 and 3
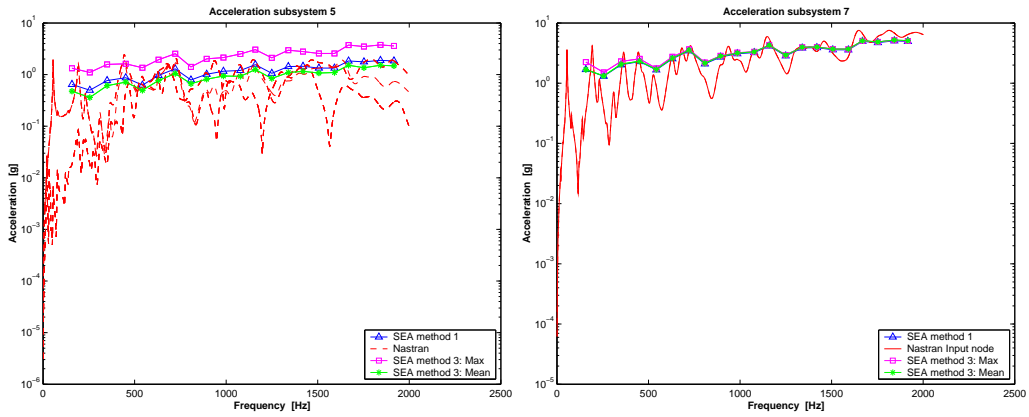
(b) Acceleration 3rd subsystem, Methods 1 and 3
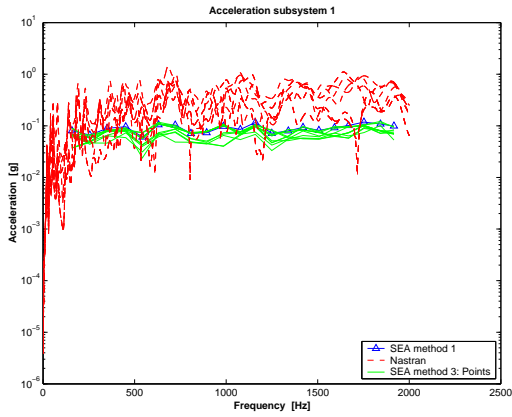
(c) Acceleration 5th subsystem, Methods 1 and 3
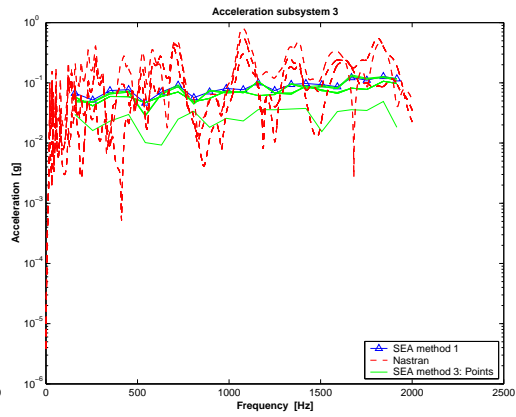
(d) Acceleration 7th subsystem, Methods 1 and 3
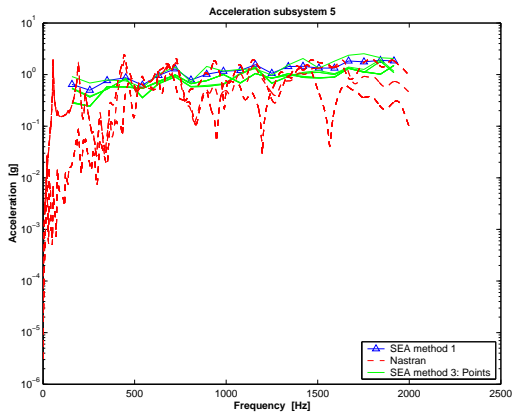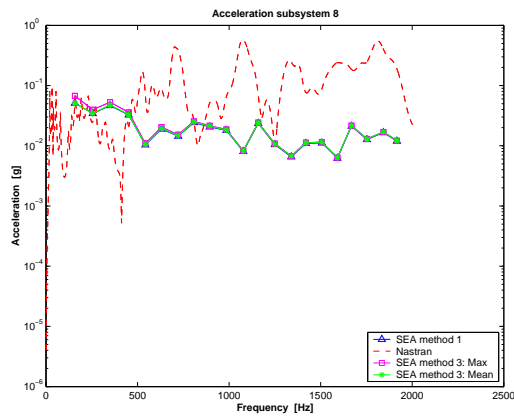
(e) Acceleration 8th subsystem, Methods 1 and 3

Figure 30: Accelerations, SD Conpare
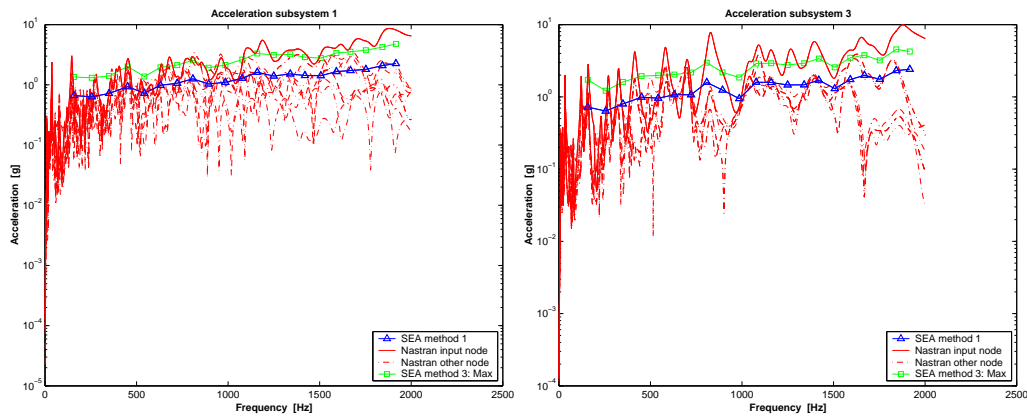
(a) Acceleration 1st subsystem, Methods 1 and 3

(b) Acceleration 3rd subsystem, Methods 1 and 3
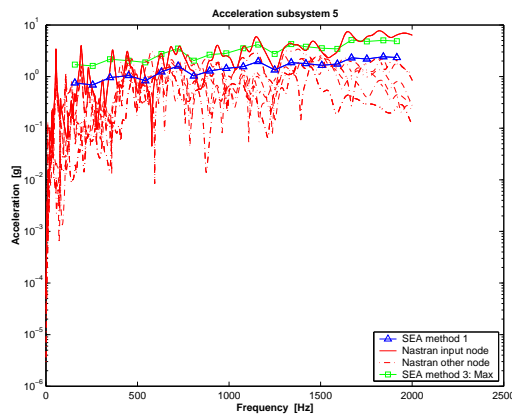
(c) Acceleration 5th subsystem, Methods 1 and 3

Figure 31: Accelerations, Power in *All* ss. in 1 point – DoF 1-6 blocked

consider the modes individually (selective distribution) so it was possible to obtain an average maximal acceleration who interpolates better the expected results. Also in this third case, all the potentialities are observable for a vibroacoustic condition where all the subsystems are stimulated; nevertheless, the method is always interesting for a microvibrations case. The solving time is short even if it is larger than the solving time of the first method.

(a) Acceleration 1st subsystem, Methods 1 and 3

(b) Acceleration 3rd subsystem, Methods 1 and 3

(c) Acceleration 5th subsystem, Methods 1 and 3
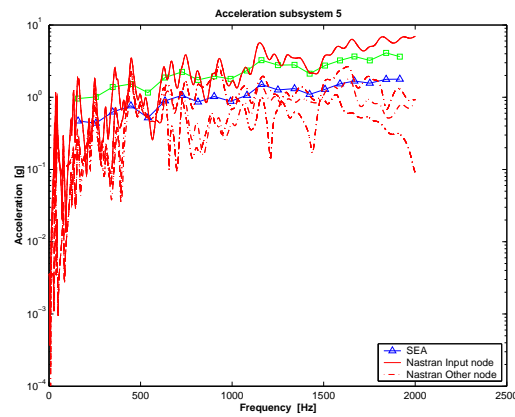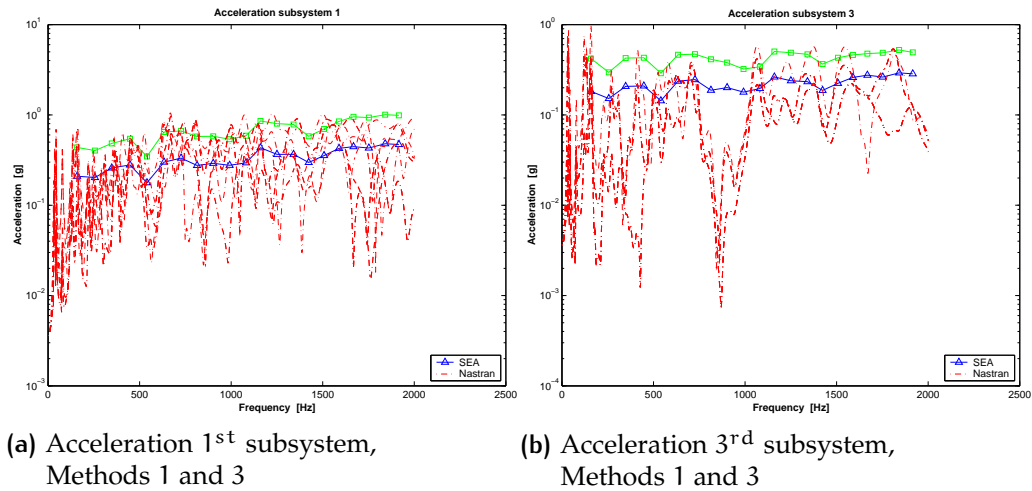
Figure 32: Accelerations, Power in 5th ss. in 1 point – DoF 1-6 blocked – Free-free configuration

4.4 FREE-FREE CONFIGURATION

All previous results were obtained with a blocked system, so the analyses were repeated with a free-free configuration to consider a situation near to reality (Fig. 32). As explained in the previous paragraph, the green line with a square marker represents the maximal acceleration in the subsystem. The type and the quality of the results do not change then, there is not influence of the limit conditions in the solving method.

Table 1: Solving time for the three methods

	Nastran [s]	1 [s]	2 [s]	3un [s]	3mM [s]	3sdM [s]
Cube 6 ss.	63.28	52.16	1077.09	62.82	146.14	146.66
Nanosat	1238.50	759.07	—	895.83	2792.90	2834.50

Legend	
1	First method (§ 4.1 on page 29)
2	Second method (§ 4.2 on page 37)
3un	Third method, uniform energy distribution (§ 4.3 on page 41)
3mM	Third method, minimal and maximal average acceleration (§ 4.3.3 on page 44)
3sdM	Third method, maximal acceleration (§ 4.3.5 on page 47)

4.5 SOLVING TIME

This section will depict the solving time of each method illustrated in the previous paragraphs. While the solving time of Nastran increases with the number of analyzed points, the solving time of the SEA method depends on the number of subsystems. Then, the SEA method becomes more interesting for big systems with a large number of points. This explains the difference of the results between the Nastran and SEA in the two models (the cube and Nanosat). The solving time of the second method (Acc2) is easily obtained by the relation: $t_{Acc2} = t_{Nastran} \cdot 3 \cdot N_{ss}$, where N_{ss} is the number of subsystems.

5 | NANOSAT

This chapter will depict the results obtained in a more complex system, Nanosat. All the considerations founded and the hypothesis used in the previous chapter will be applied in this new model.

5.1 MODEL'S PREPARATION

The model for the SEA analysis was based on the needed condition found in the previous analyses. Then, a correct number of modes for band, a correct number of points for subsystem and a right maillage were researched (see § 3.2.4 on page 24). A good choice of these three factors is important, in fact, an analysis with a bad maillage was carried out and bad results were obtained. The choice of the subsystems can influence the results, hence, the more plausible configuration was chosen, as in showed in Fig. 33 on the next page.

5.2 ANALYSES AND RESULTS

In the first analysis, a blocked model in the first subsystem was considered and also the power was injected in the subsystem 1 (Fig. 34, 35 and 36). Not according to it was expected, the acceleration of the first subsystem is very different from the accelerations obtained with the sinus analysis, whereas, the SEA acceleration result of the other subsystems in the little-system *caisson* is more acceptable. As expected the acceleration's trend of each subsystem is similar to the acceleration of the first subsystem. While this trend could be correct or similar for the subsystems of the
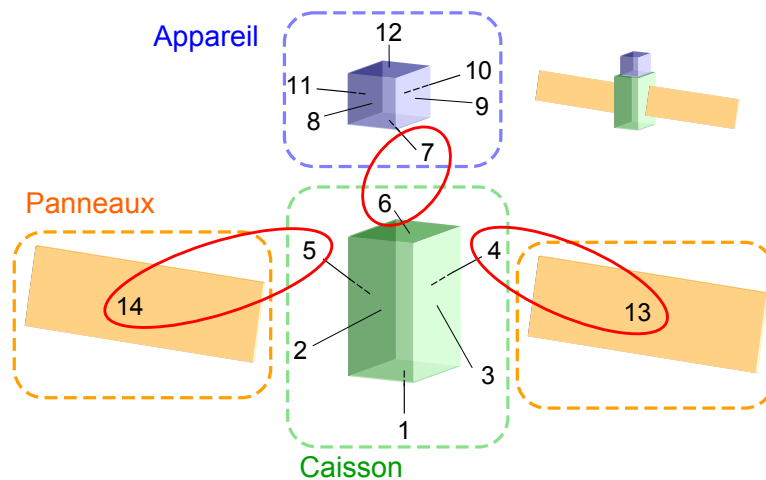
Figure 33: Nanosat model

caisson it becomes completely different for the other little-systems (*appareil* and *panneaux*).

Despite of the different acceleration between the SEA and the sinus analysis, the total energy is equal in the two methods. Nevertheless, the total energy matches in the two cases only starting at 1000 Hz (Fig. 37 on page 62). A possible explanation will be presented in the next paragraph.

In the previous chapter the influence of a supple subsystem was detected (see § 4.1.2) so harder springs who connect the *appareil* to the *caisson* were taken (Fig. 38, 39 and 40 on pp. 63-65). In spite of, the quality of solution was not changed however, a better trend of the total energy appear as observable in Fig. 41 on page 65. Hence, the presence of a supple subsystem can interfere on the results. Anyhow, another way to ameliorate the solution must be found.

The same model was analysed in free-free condition (Fig. 42, 43 and 44 on pp. 66-68), a little refinement of the results appear but they have the same errors on the *appareil* and *panneaux* little-systems.

The problem of results not completely correct for the little-systems *appareil* and *panneaux* was analyzed, and the solution was identified in a localization of the power. More analyses were necessary for the correction of the results; first, an input power was injected in the first subsystem as in the previous cases. Then, the net power flows were calculated and three further analyses were actuated. In these three analyses a net power flows between the *caisson* and the *appareil* little-systems and between the *caisson* and the *panneaux* little-systems were injected in the system to obtain new results. In particular, the net power flow between the subsys-

tems $6 - 7$ was injected in the subsystem 7, the net power flow between the subsystems $5 - 14$ was injected in the subsystem 14 and, at the same way, between the subsystems $4 - 13$ in the 13th. With this correction a better solution can be observed as showed in Fig. 46 and 47 on pp. 69-70. Clearly, the total energy of the SEA and of the sinus analysis is not equal anymore. The disadvantage is that three further analyses are necessary, hence a larger solving time.

Despite the solution with only one subsystem solicited is not completely correct, the solution for the acoustic case is correct, as can be observed in Figures 48-50 on pp. 71-73. The blue line represents the SEA solution with the first method, while the green line represents the maximal acceleration (not the average maximal acceleration) obtained with the third method.

(a) Acceleration 1st subsystem

(b) Acceleration 2nd subsystem

(c) Acceleration 3rd subsystem

(d) Acceleration 4th subsystem

(e) Acceleration 5th subsystem

(f) Acceleration 6th subsystem
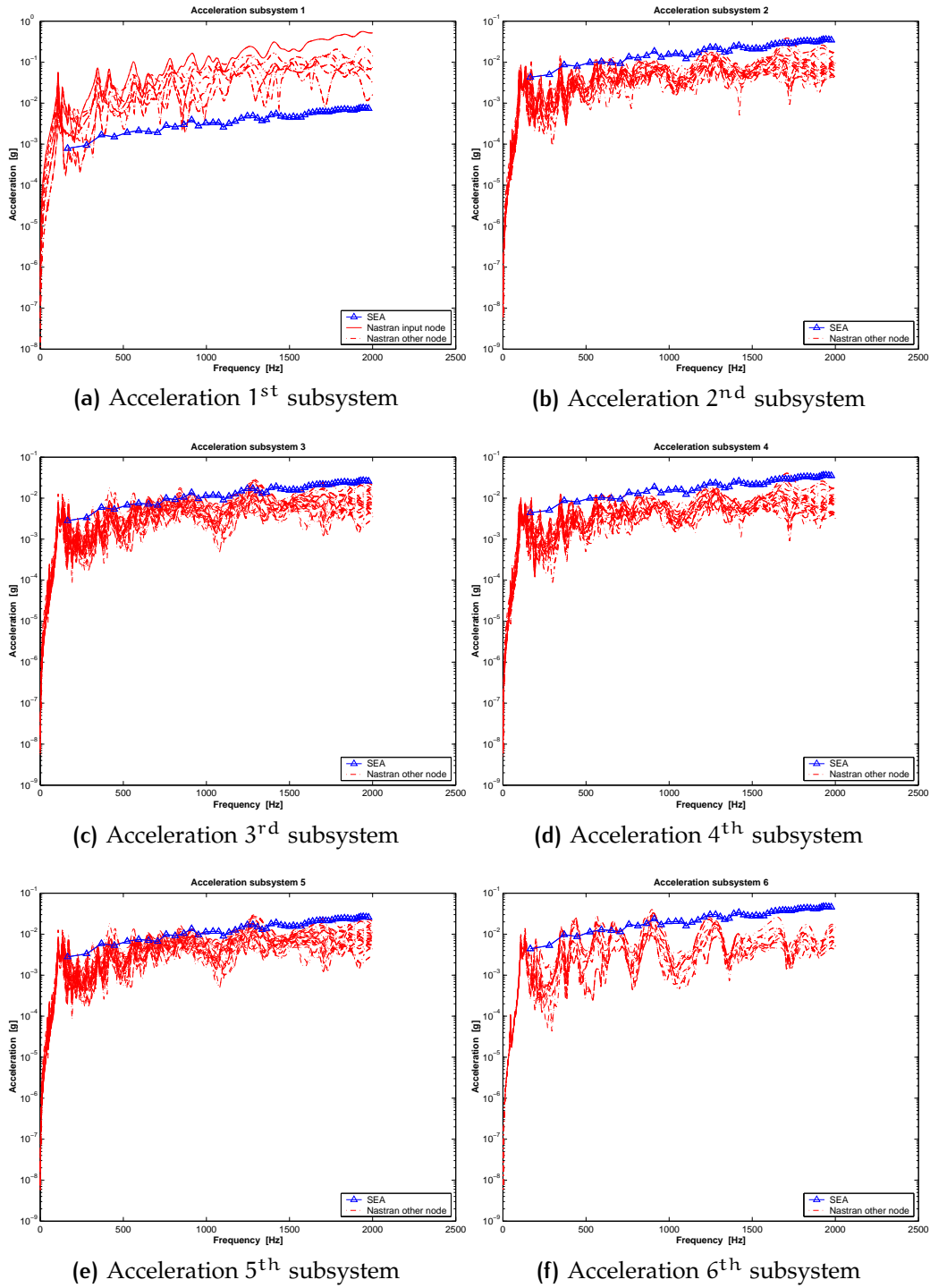
Figure 34: Initial – Caisson

(a) Acceleration 7th subsystem

(b) Acceleration 8th subsystem

(c) Acceleration 9th subsystem

(d) Acceleration 10th subsystem

(e) Acceleration 11th subsystem

(f) Acceleration 12th subsystem
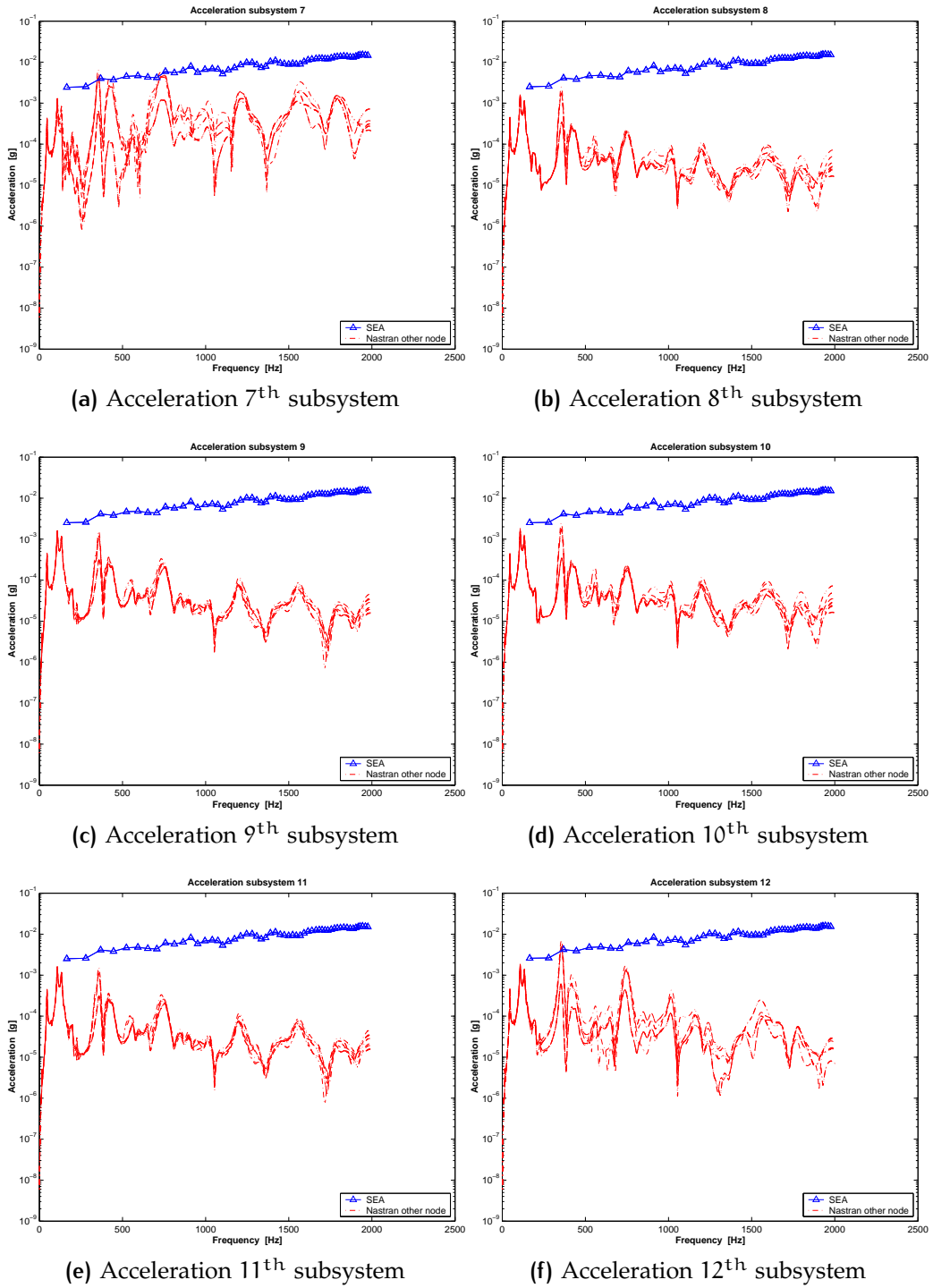
Figure 35: Initial – Appareil

(a) Acceleration 13th subsystem   **(b)** Acceleration 14th subsystem
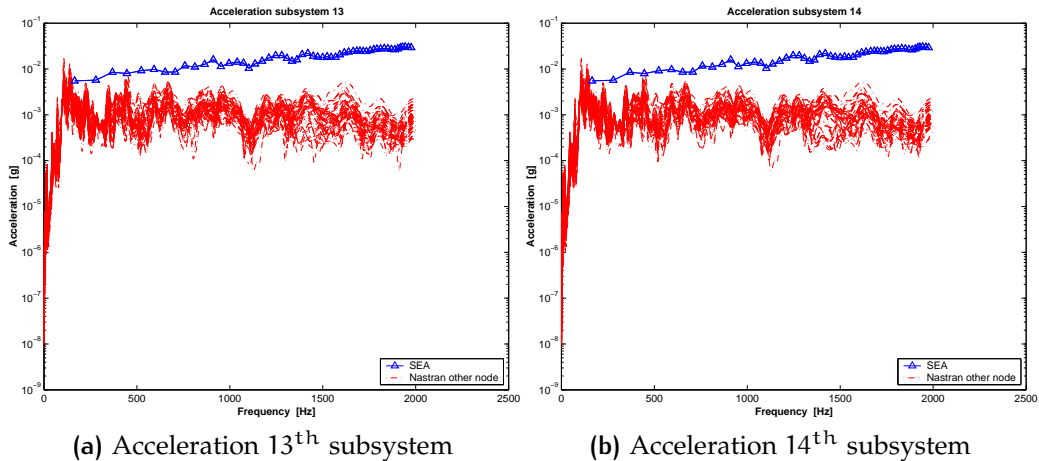
Figure 36: Initial – Panneaux
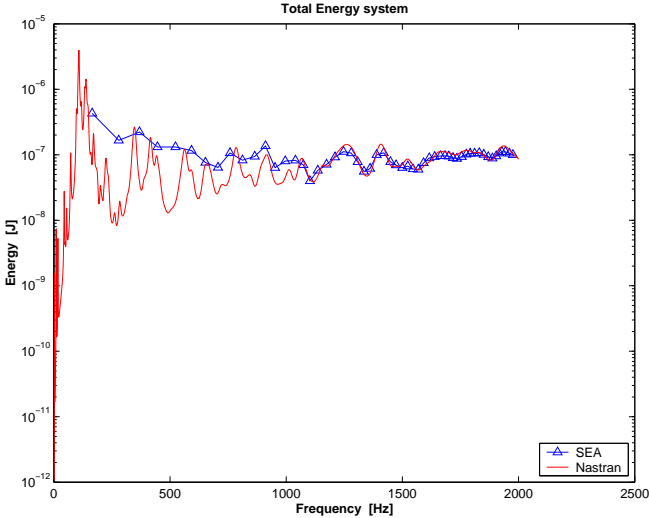
Figure 37: Initial – Total energy

(a) Acceleration 1st subsystem

(b) Acceleration 2nd subsystem

(c) Acceleration 3rd subsystem

(d) Acceleration 4th subsystem

(e) Acceleration 5th subsystem

(f) Acceleration 6th subsystem
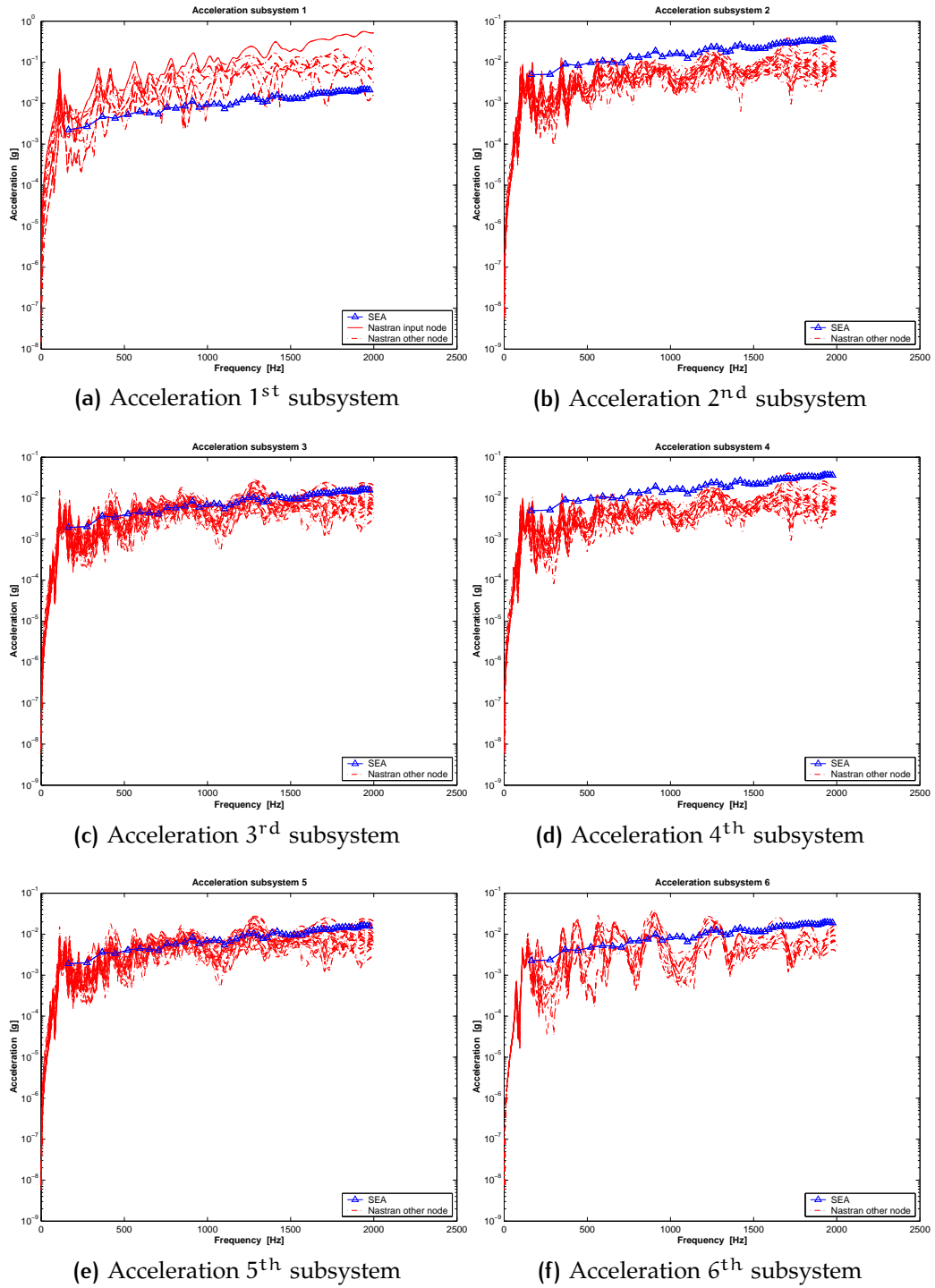
Figure 38: Bigger K spring – Caisson

(a) Acceleration 7th subsystem

(b) Acceleration 8th subsystem

(c) Acceleration 9th subsystem

(d) Acceleration 10th subsystem

(e) Acceleration 11th subsystem

(f) Acceleration 12th subsystem
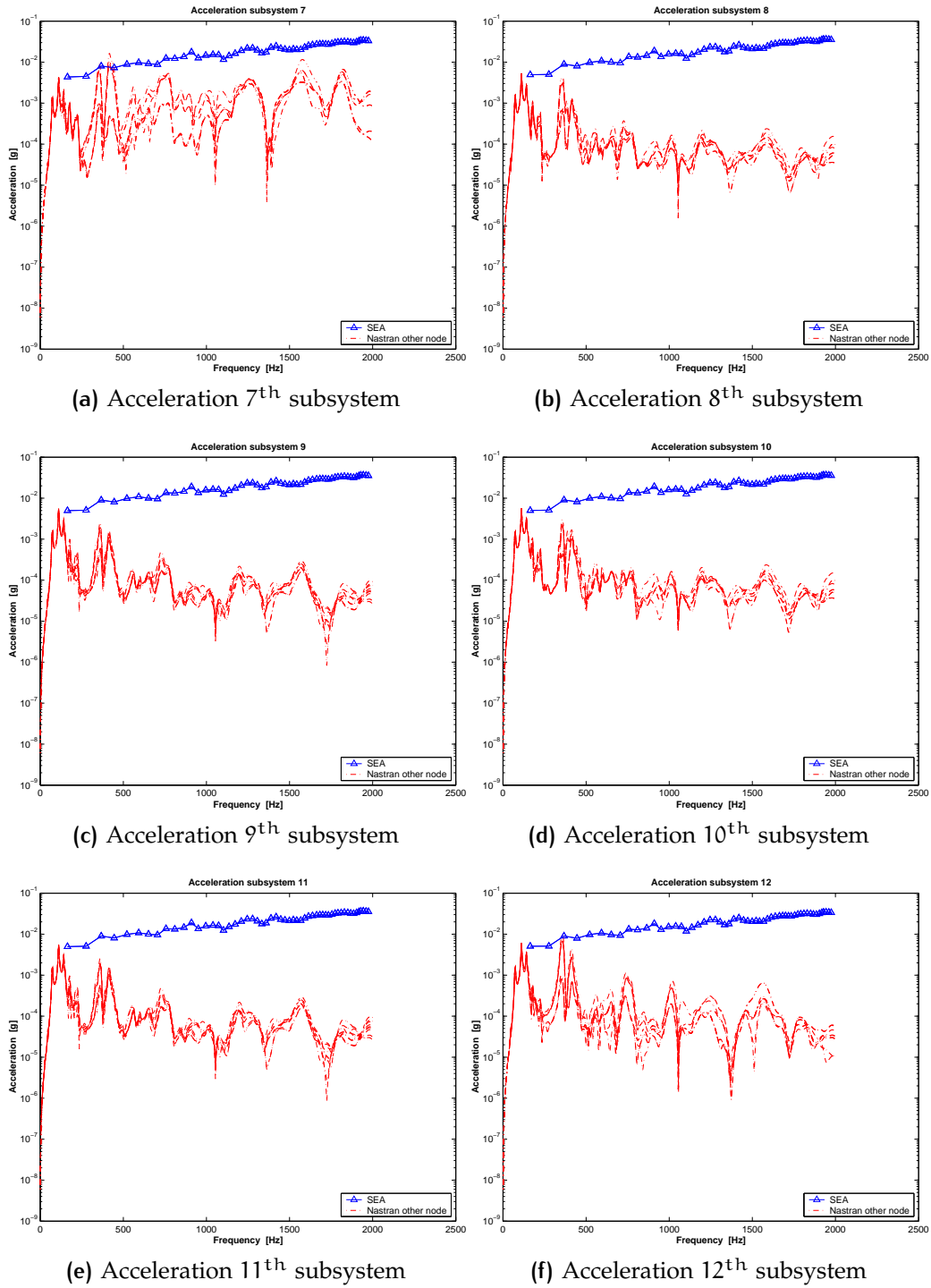
Figure 39: Bigger K spring – Appareil

(a) Acceleration 13$^{\text{th}}$ subsystem

(b) Acceleration 14$^{\text{th}}$ subsystem
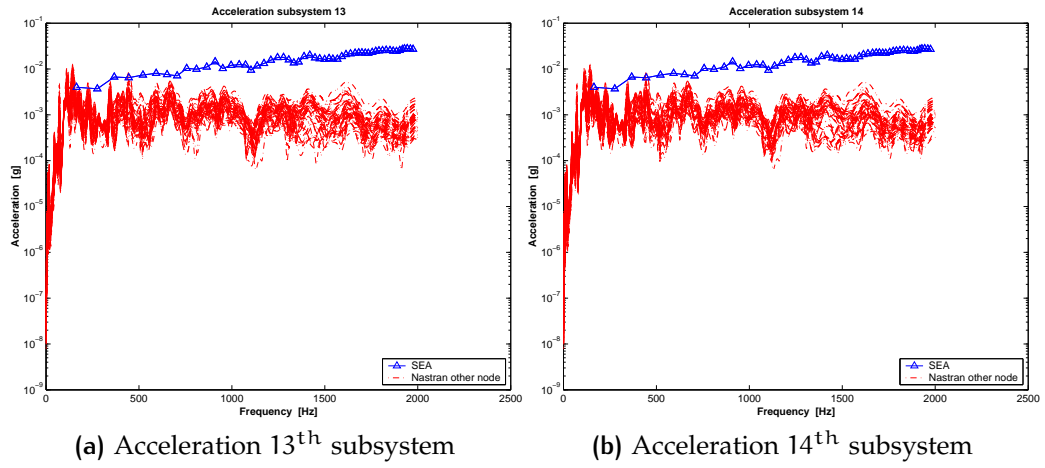
Figure 40: Bigger K spring – Panneaux
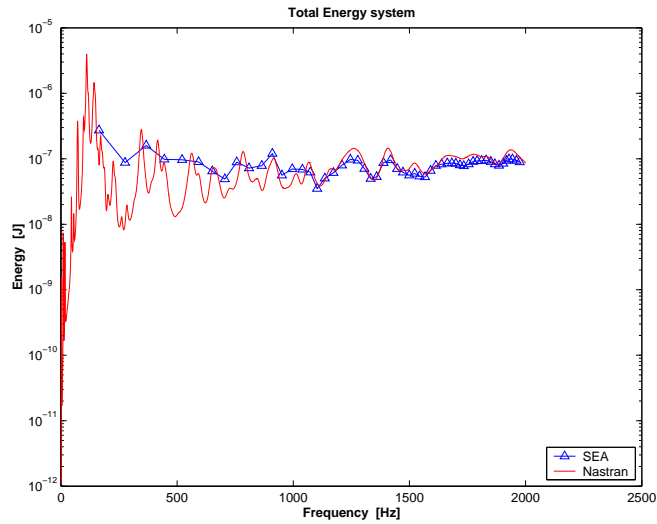
Figure 41: Bigger K spring – Total energy

(a) Acceleration 1st subsystem

(b) Acceleration 2nd subsystem

(c) Acceleration 3rd subsystem

(d) Acceleration 4th subsystem

(e) Acceleration 5th subsystem

(f) Acceleration 6th subsystem
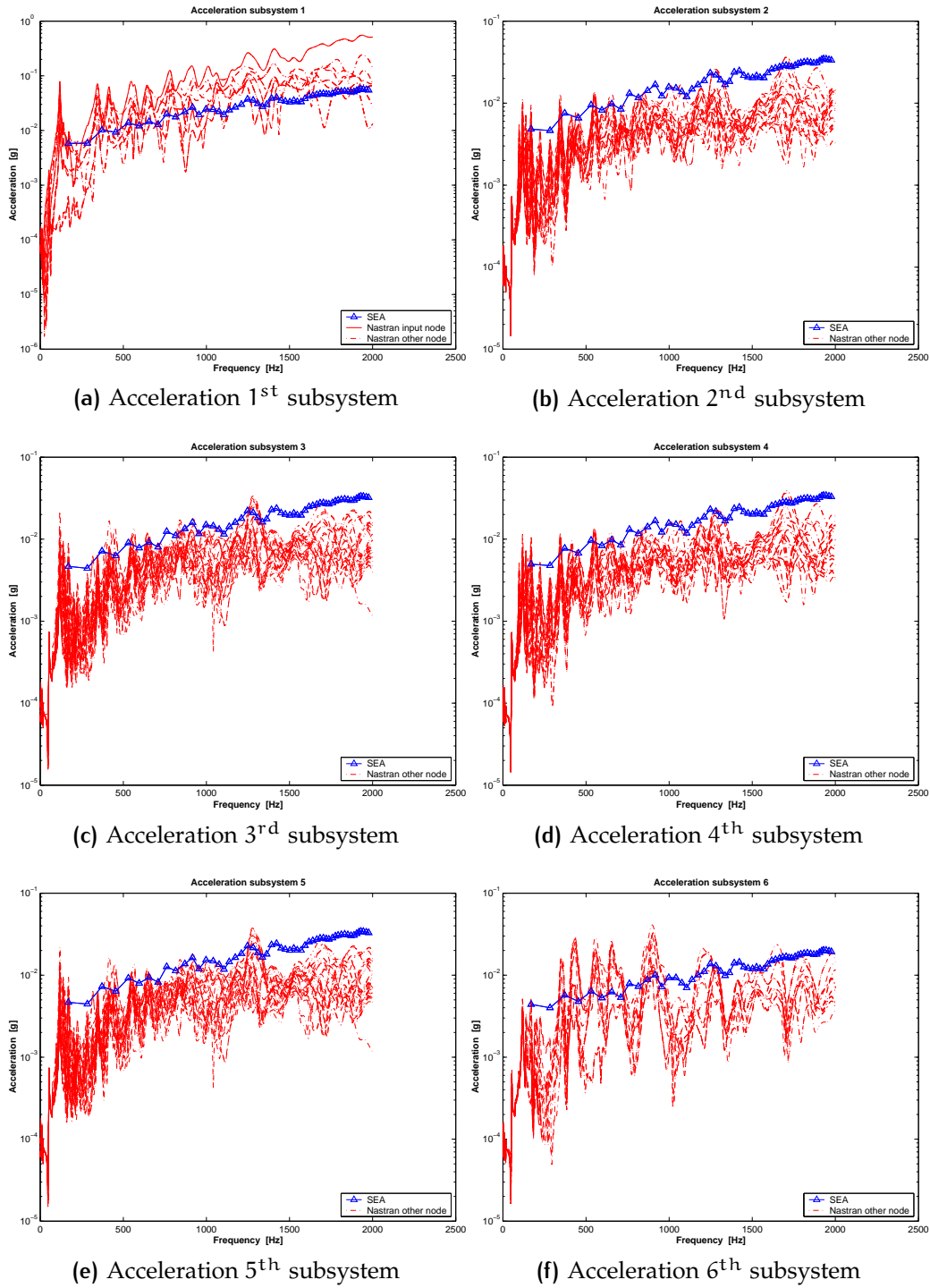
Figure 42: Free-free configuration – Caisson

(a) Acceleration 7th subsystem

(b) Acceleration 8th subsystem

(c) Acceleration 9th subsystem

(d) Acceleration 10th subsystem

(e) Acceleration 11th subsystem

(f) Acceleration 12th subsystem
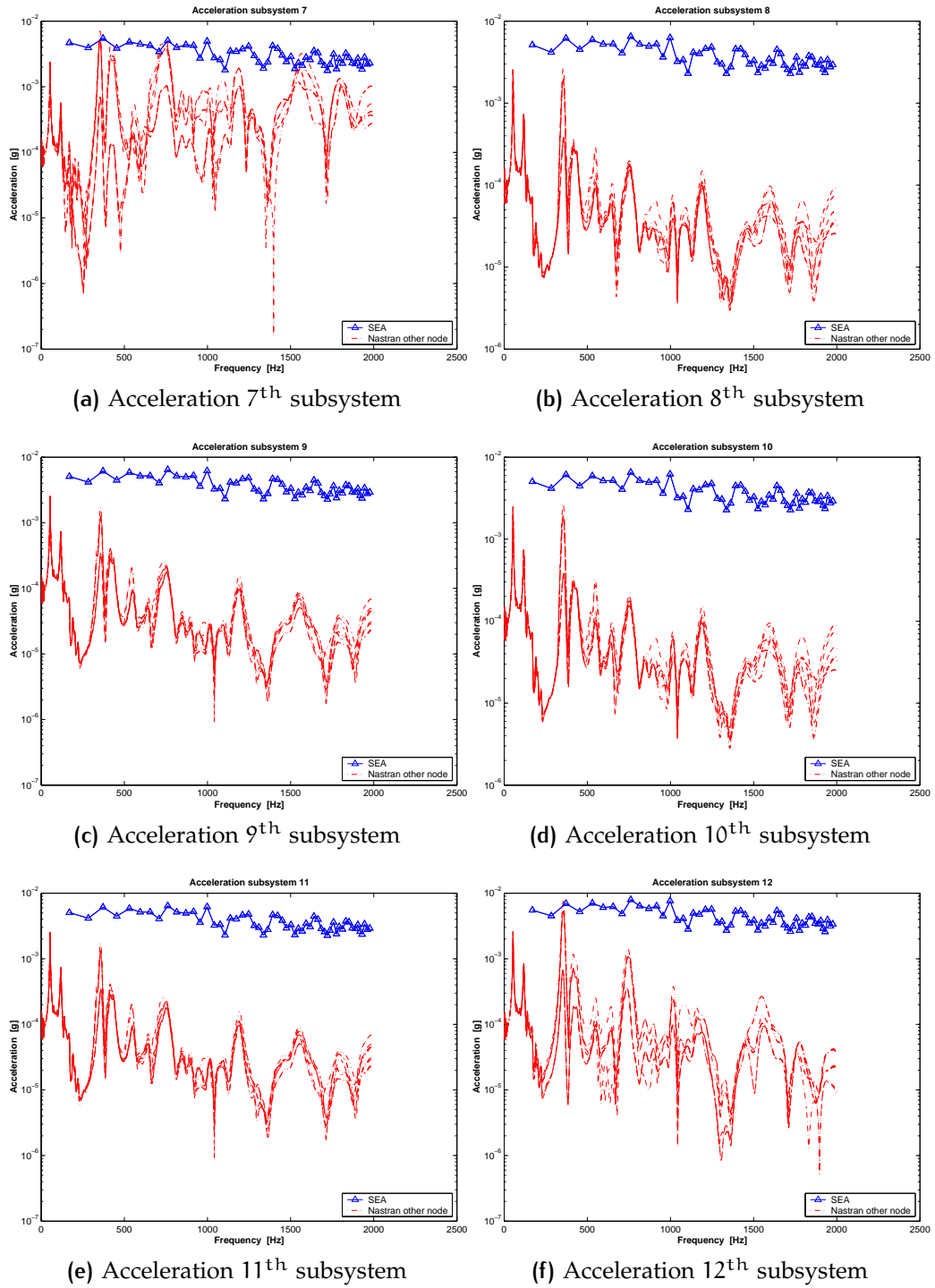
Figure 43: Free-free configuration – Appareil

(a) Acceleration 13$^{\text{th}}$ subsystem

(b) Acceleration 14$^{\text{th}}$ subsystem
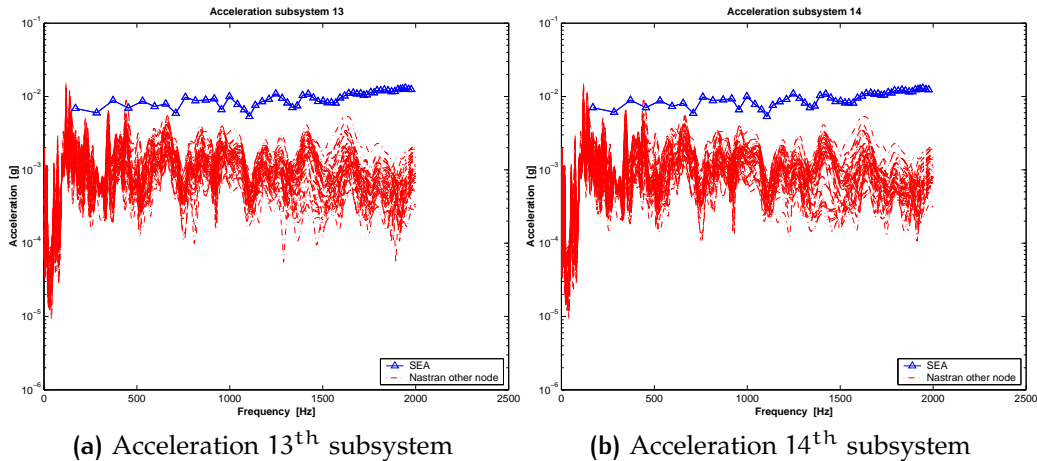
Figure 44: Free-free configuration – Panneaux
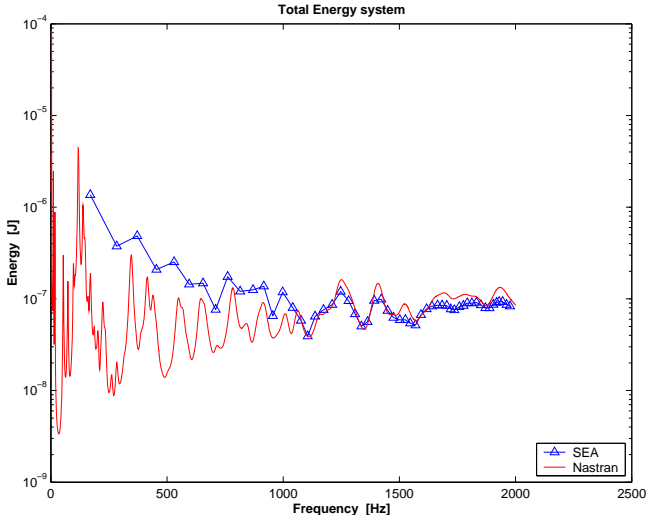
Figure 45: Free-free configuration – Total energy

(a) Acceleration 7th subsystem

(b) Acceleration 8th subsystem

(c) Acceleration 9th subsystem

(d) Acceleration 10th subsystem

(e) Acceleration 11th subsystem

(f) Acceleration 12th subsystem
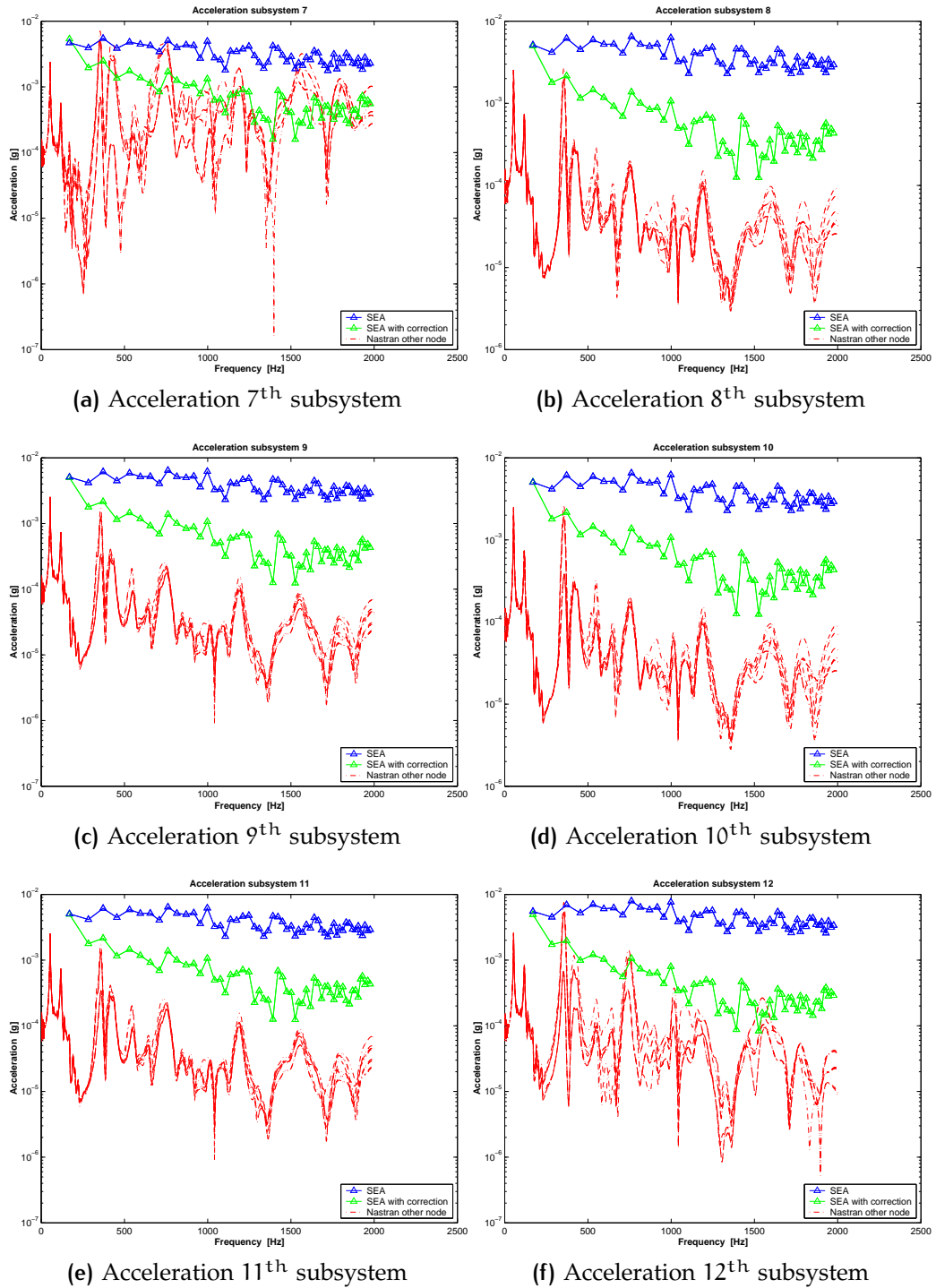
Figure 46: Free-free configuration with correction – Appareil
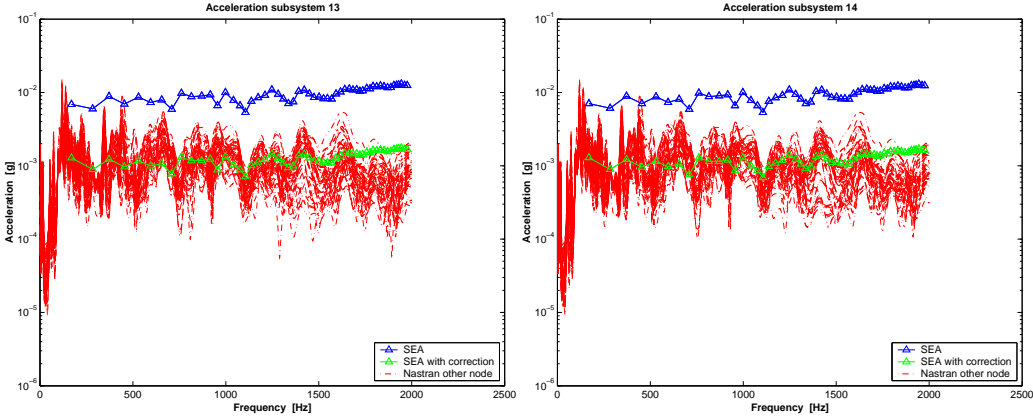
(a) Acceleration 13th subsystem

(b) Acceleration 14th subsystem

Figure 47: Free-free configuration with correction – Panneaux
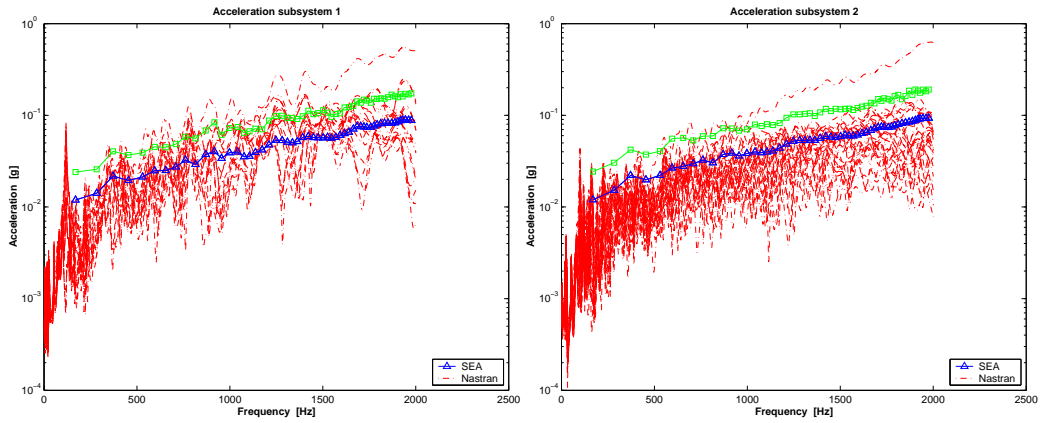
(a) Acceleration 1st subsystem
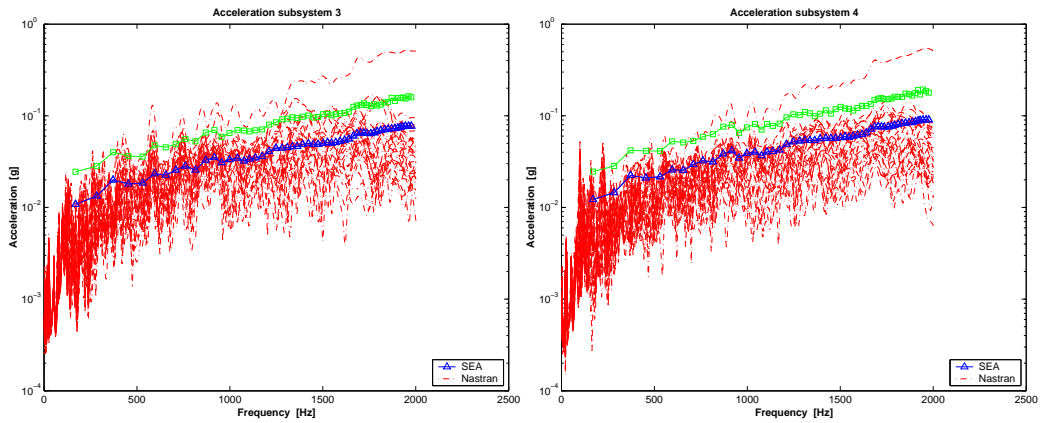
(b) Acceleration 2nd subsystem

(c) Acceleration 3rd subsystem

(d) Acceleration 4th subsystem
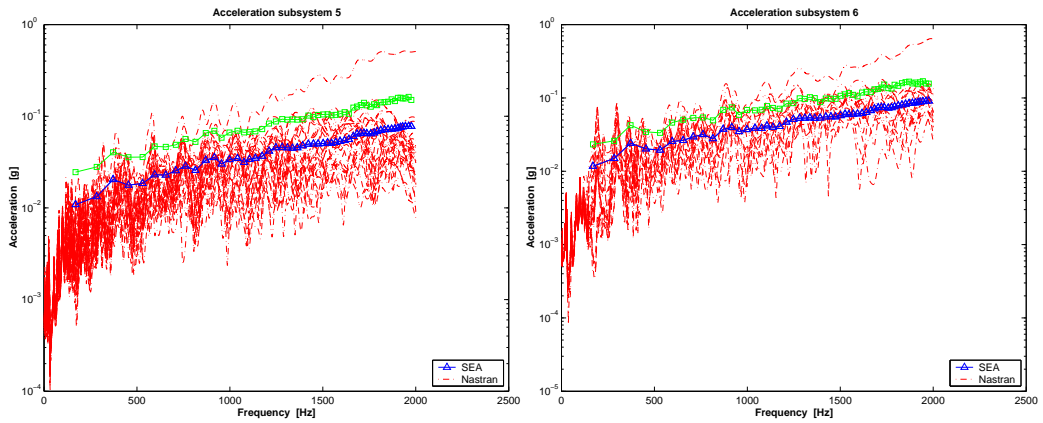
(e) Acceleration 5th subsystem

(f) Acceleration 6th subsystem

Figure 48: Free-free configuration, Power in *All* ss. – Caisson
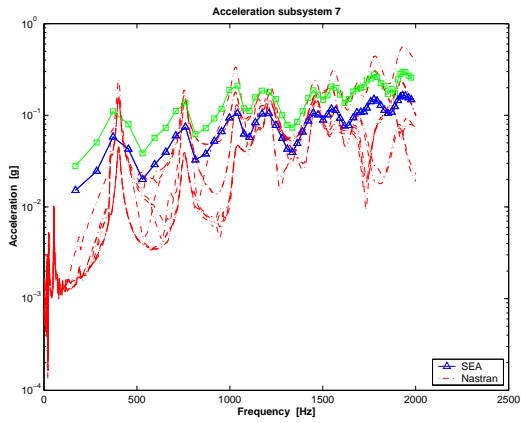
(a) Acceleration 7th subsystem
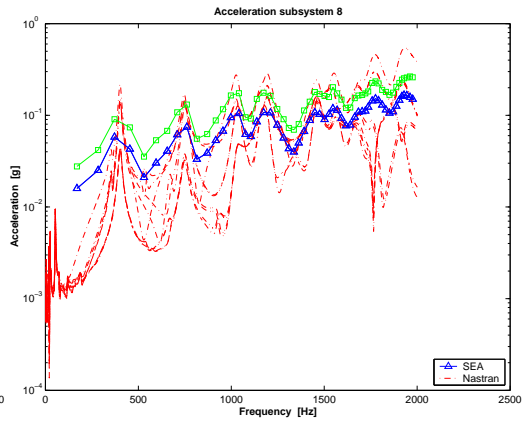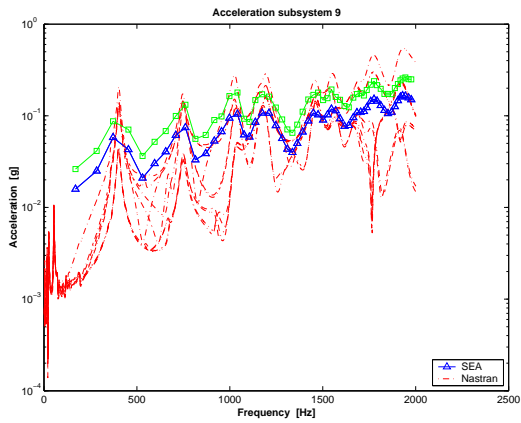
(b) Acceleration 8th subsystem

(c) Acceleration 9th subsystem
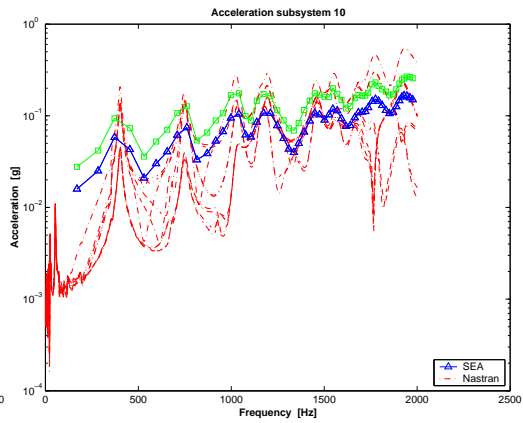
(d) Acceleration 10th subsystem
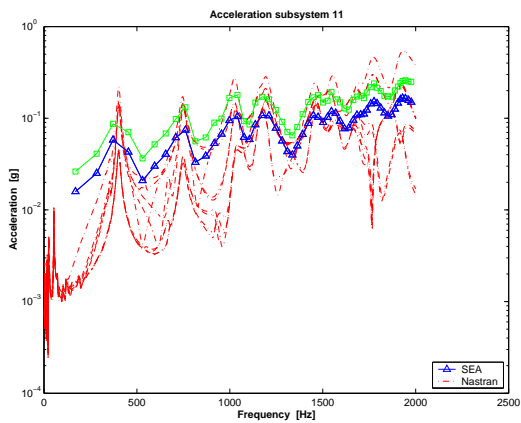
(e) Acceleration 11th subsystem
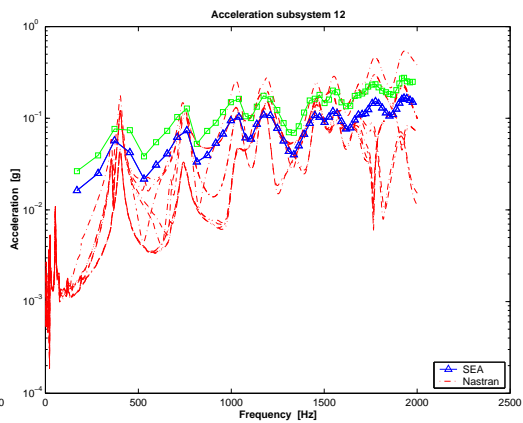
(f) Acceleration 12th subsystem

Figure 49: Free-free configuration, Power in *All* ss. – Appareil
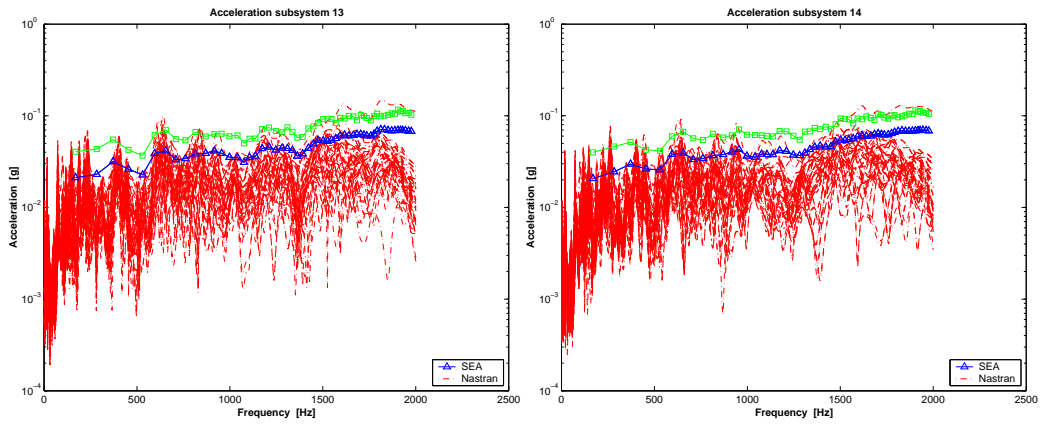
(a) Acceleration 13th subsystem

(b) Acceleration 14th subsystem

Figure 50: Free-free configuration, Power in *All* ss. – Panneaux

A | MATLAB CODE

This section will depict the Matlab code developed for the Quasi-SEA. The principal functions are the `SEA_FE` and `acc_mat` that evaluate the principal elements of the sea method and the acceleration of the subsystems.

A.1   SEA_FE

This function evaluates all elements of the SEA method such as the *energy* for each frequency range and for each subsystem, and the *net power flows*. The syntax of the function is the following:

```
1  [F,A,E] = SEA_FE(file_pch,file_nodes,M,N,Nmode,P)
2  [F,A,E] = SEA_FE(file_pch,file_nodes,M,N,Nmode,P,fre_P,Pss)
3
4  [F,A,E,Nodes] = SEA_FE(file_pch,file_nodes,M,N,Nmode,P)
5  [F,A,E,NFvec,NFmat,leg] = SEA_FE(file_pch,file_nodes,M,N,Nmode,P)
```

A.1.1   Input elements

FILE_PCH : address where the file *.pch* is available (e.g. `/dideas30/SEA/ stagehp/RESULTS/MODAL/`*name*`.pch`).

FILE_NODES: address where the file *.dat* or *.txt* is available. For more details see the parameter N. (e.g. `/dme/SEA/stagehp/DAT/MODAL/` *name*`.dat`).

M: row vector with the mass in kg of each subsystem.

N: number of points for the subsystems. There are two different cases:

- **N** = $n > 0$: n random points are analysed, obteined by *name.txt* in `file_nodes`. In the file *name.txt* all points of the subsystems must be present assembled in rows, each row in the file corresponds to a subsystem.

- **N** = -1: *all* points obtained by *name.dat* or *name.txt* in `file_nodes` are analysed. Each row in the file corresponds to a subsystem. The nuber of points in the rows can be different for each subsystem.

NMODE: number of modes for each frequency range ($Nmode > 0$).

For the input power there are two options, *constant* or *not constant* input power:

CONSTANT `[...]` = `SEA_FE(...,P)`, `P` is a column vector with the input power in W for each subsystem (e.g. if `P = [0 0 1 0]'` then, only a constant input power of $1W$ is injected in the 3rd subsystem)

NOT CONSTANT `[...]` = `SEA_FE(...,P,fre_P,Pss)`, `P` is a matrix $m \times n$ where the ith column contains the value of power at `freq_P` injected in the subsystem written in the ith column of `Pss`. (e.g. `P = [P_a P_b P_c]`; `Pss = [2 5 1]`, the power `P_a` is injected in the subsystem 2, `P_b` in the subsystem 5 and `P_c` in the subsystem 1). `freq_P` is a column vector $m \times 1$. The values of power between two frequencies (e.g. `P(fre_P(i))` and `P(freq_P(i+1))`) is obtained by a linear interpolation, then a small pace is suggested.

A.1.2 Output elements

F: frequency in Hz at the borders of the frequency bands. If 20 frequency bands were analysed between $200 - 1000 \, \text{Hz}$, then F is a column vector 1×21, $F = [200 : \frac{1000-200}{20} : 1000]$.

A: it is a 3D matrix $n \times n \times m$ where n is the number of subsystems and m is the number of frequency bands. (§ 2.1 on page 11)

E: energy of the subsystems in J; it is a matrix $m \times n$, where n is the number of subsystems and m is the number of frequency bands. Hence, $E(1,2)$ is the energy of subsystem 1 in the 2nd range. (§ 2.1 on page 11)

NODES: matrix $n \times N$ with the list of points chosen for each subsystem. n is the number of subsystems and N is the maximal number of points chosen for the subsystems. Some elements of the matrix could be zero.

NFVEC: net power flow between the subsystems; it is a matrix $p \times m$, where m is the number of frequency bands and $p = \frac{n(n-1)}{2}$ is the nuber of all possible combinations of flows between the subsystems, with n the number of subsystems. The net power flow of the row i^{th} is described in the row i^{th} of leg.

NFMAT: net power flow between the subsystems; it is a 3D matrix $n \times n \times m$ where n is the number of subsystems and m is the number of frequency bands. The net power flow in position (r,s) is the net power between the subsystems r and s. (§ 3.1.2 on page 20)

LEG: it is a row vector of string, with the legend to read NFvec.

A.1.3 Examples

Two examples of application of the function will be depicted.

Example 1

In the first example, the energies of the subsystems obtained when a constant input power of $1\,W$ is injected in the 5th subsystem will be represented.

```
6     P = [0 0 0 0 1 0]';              % Power introduced
7
8     Sf = [1 1 1 1 1 1]*0.75*0.75;   % Surfaces
9     t = [3 3 3 3 3 3]*1e-3;         % Thickness
10    rho = [1 1 1 1 1 1]*2800;       % Density
11    M = Sf.*t.*rho;                 % Mass
12
13    % Data file
14    name_f = 'cubegen';
15    namef_pch = ['/dideas30/SEA/stagehp/RESULTS/MODAL/',name_f,'.pch'];
16    namef_dat = ['/dme/SEA/stagehp/DAT/MODAL/',name_f,'.dat'];
17
```

```
18    % SEA resolution
19    [F,A,E] = SEA_FE(namef_pch,namef_dat,M,-1,35,P);
20
21    % Frequency
22    f = (F(1:end-1) + F(2:end))/2;
23
24    % Image
25    figure(1)
26    semilogy(f,E,'LineWidth',2)
27    legend('subsys 1','subsys 2','subsys 3','subsys 4','subsys 5','subsys 6'
             )
28    title('Energy subsystems','FontWeight','bold')
29    xlabel('Frequency  [Hz]'); ylabel('Energy   [J]')
30    grid
```

Example 2

In the second example a non-constant power is injected in the 5th subsystem. Then, the net power flow will be plotted in two figures. In figure two only the net power flows of the first frequency range are plotted (range_ana = 1), whereas in the first figure all net power flows in all bands are plotted.

```
31    name_f = 'cubegen';
32    namef_pch = ['/dideas30/SEA/stagehp/RESULTS/MODAL/',name_f,'.pch'];
33    namef_dat = ['/dme/SEA/stagehp/DAT/MODAL/',name_f,'.dat'];
34
35    addpath /dme/fortran/larue/MATLAB/read_pch_s103/v1
36    modale_syst = read_pch_s103(namef_pch);
37
38    spectre = [1 1 2000 1];
39    spectre = reshape(spectre',2,length(spectre)/2)';
40    freq1 = [1. 1. 2000.];
41    freq4 = [1. 2000. 0.1 1];
42    Q_cst = [  -0.10   25. ; ...
43               500.    25.];
44
45    % Input power
46    microvib_fz = [];
47    microvib_fz = sol_111_SEA( modale_syst , [1985 3 1] , spectre ,...
48                freq1 , freq4 , Q_cst , 'VELO',[1985]);
49    P(:,1) = (microvib_fz(1).amp(:,1).^2+microvib_fz(1).amp(:,2).^2+...
50                microvib_fz(1).amp(:,3).^2).^0.5;
51    fre_P = microvib_fz(1).freq(:,1);
52
53    % SEA
54    Sf = [1 1 1 1 1 1]*0.75*0.75;  % surfaces
55    t = [3 3 3 3 3 3]*1e-3;        % thickness
```

```matlab
56      rho = [1 1 1 1 1 1]*2800;        % density
57      M = Sf.*t.*rho;
58      [F_range,A,E_sea,NF_vec,NF_mat,leg] = SEA_FE(namef_pch,namef_dat,M
            ,-1,...
59                      35,P,fre_P,5);
60
61      % Frequency
62      f = (F(1:end-1) + F(2:end))/2;
63
64      % Images
65      figure(1)
66      plot(NF_vec')
67      title('Net Power flow','FontWeight','bold');
68      xlabel('Range','FontWeight','bold');
69      ylabel('Power flow  [W]','FontWeight','bold');
70      legend(leg)
71
72      figure(2)
73      range_ana = 1;
74      W_ana = NF_mat(:,:,range_ana);
75      for j =1:6
76              W_ana(j,j) = nan;
77      end
78      h = bar3(W_ana);
79      xlabel('Subsystem - s');
80      ylabel('Subsystem - r');
81      title(['Net Power Flow r -> s : f = ',num2str(ceil(f(range_ana))),' Hz'
            ])
82      v = 6;
83      for i = 1:length(h)
84          zdata = ones(v*length(h),4);
85          k = 1;
86          for j = 0:v:(v*length(h)-v)
87              zdata(j+1:j+v,:) = W_ana(k,i);
88              k = k+1;
89          end
90          set(h(i),'Cdata',zdata)
91      end
92      colormap jet
```

A.2   ACC_MAT

This function evaluates, with three different methods, the accelerations of each subsystem by the characteristics of the subsystems obtained by SEA. The syntax of the function is the following:

```matlab
93      acc1 = acc_mat('acc_ana_1',E,F,M);
```

```
94    acc2 = acc_mat('acc_ana_2',namef_pch,F,E,Nodes);
95    acc3 = acc_mat('acc_ana_3',namef_pch,F,E,Nodes,M,dis);
```

A.2.1 Input elements

ACC_ANA_1: evaluation of the acceleration by method 1, *direct acceleration* (§ 4.1 on page 29).

ACC_ANA_2: evaluation of the acceleration by method 2, *acceleration by mobility* (§ 4.2 on page 37).

ACC_ANA_3: evaluation of the acceleration by method 3, *acceleration by α_j* (§ 4.3 on page 41).

DIS type of energy distribution

> **DIS** = 0: uniform energy's distribution, each mode has the same quantity of energy;
>
> **DIS** = n: the energy of the band is concetrated in the nth mode of the band.
>
> **DIS** = −1: the energy of the band is concentrated in each mode in sequential way. The maximal and minimal average acceleration for each frequency band is extrapolated. An example of results is in Fig. 25 on page 48. (see § A.2.2 for a correct use of the output parameters)
>
> **DIS** = −3: the energy of the band is concentrated in each mode in sequential way. The maximal (*not* average) acceleration for each frequency band is extrapolated. An example of results is in Fig. 30 on page 53.

For the meaning of the others input elements see § A.1.1 and § A.1.2 on page 76.

A.2.2 Output elements

ACC1/ACC2/ACC3: acceleration in g of each subsystem and for each frequency band. It is a matrix $m \times n$, where n is the number of subsystems and m is the number of frequency bands.

Nota for acc2

If the parameter $dis = -1$ was chosen to calculate the acceleration with the method 2 then a different output parameter is generated. In fact, in this case the parameter $acc2$ is not a matrix $m \times n$ but a 3D matrix of dimensions: $m \times n \times 4$. The matrix in position 1 ($m \times n \times 1$) contains the minimal acceleration and in position 3 ($m \times n \times 3$) the frequencies f_n of the modes which produce it. At the same way, in positions 2 ($m \times n \times 2$) and 4 ($m \times n \times 4$) the maximal acceleration and the frequency of the modes linked can be found.

A.2.3 Exemple

One example of application of the function.

```
96   P = [0 0 0 0 1 0]';              % Power introduced
97   Sf = [1 1 1 1 1 1]*0.75*0.75;    % Surfaces
98   t = [3 3 3 3 3 3]*1e-3;          % Thickness
99   rho = [1 1 1 1 1 1]*2800;        % Density
100  M = Sf.*t.*rho;                  % Mass
101  % Data file
102  name_f = 'cubegen';
103  namef_pch = ['/dideas30/SEA/stagehp/RESULTS/MODAL/',name_f,'.pch'];
104  namef_dat = ['/dme/SEA/stagehp/DAT/MODAL/',name_f,'.dat'];
105  % SEA resolution
106  [F,A,E,Nodes] = SEA_FE(namef_pch,namef_dat,M,-1,35,P);
107  % Frequency
108  f = (F(1:end-1) + F(2:end))/2;
109  % Accelerations
110  % --- Method 1
111  acc1 = acc_mat('acc_ana_1',E_sea,F_range,M);
112  % --- Method 2
113  acc2 = acc_mat('acc_ana_2',namef_pch,F_range,E,Nodes);
114  % --- Method 3
115  acc3_0 = acc_mat('acc_ana_3',namef_pch,F,E,Nodes,M,0);
116  acc3_1 = acc_mat('acc_ana_3',namef_pch,F,E,Nodes,M,1);
117  % Image
118  figure(1)
119  semilogy(f,acc1(:,1),'b-^',f,acc2(:,1),'r-*',f,acc3_0(:,1),'k-o',...
120           f,acc3_1(:,1),'m-o')
121  legend('Method 1','Method 2','Method 3 Uniform energy',...
122         'Method 3 Energy mode 1');
123  title(['Acceleration subsystem ' num2str(j)],'FontWeight','bold');
124  xlabel('Frequency  [Hz]','FontWeight','bold');
125  ylabel('Acceleration  [g]','FontWeight','bold');
```

B | CHOICE OF THE POINTS
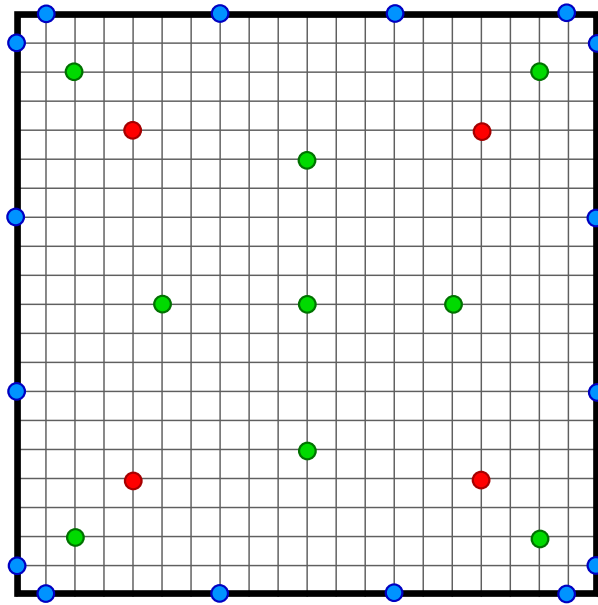
Figure 51: Rappresentation of the position of the points

In Fig. 51 the position of the characteristic points is shown. The points are classified by colour:

RED: position of the blocks, it is valid only for the 5th subsystem;

GREEN: position of the points observed to apply the sea method;

BLUE: position of the bolts, it is valid only for the 3rd subsystem and for the edges shared with the subsystems 1, 2, 4 and 6.

C | EADS ASTRIUM

The European Aeronautic Defence and Space Company N.V. (EADS) is a large pan-European aerospace corporation, formed by the merger on 10 July 2000 of DaimlerChrysler Aerospace AG (DASA) of Germany, Aérospatiale-Matra of France, and Construcciones Aeronáuticas SA (CASA) of Spain. The company develops and markets civil and military aircraft, as well as communications systems, missiles, space rockets, satellites, and related systems.

The divisions of EADS are: Airbus, Airbus Military, Astrium, EADS Defence & Security and Eurocopter.

C.1   ASTRIUM

Astrium is a wholly owned subsidiary of EADS, a global leader in aerospace, defence and related services.

Number 1 in Europe and n. 3 worldwide, Astrium employs 15,000 men and women in five countries: France, Germany, UK, Spain and the Netherlands. Guaranteeing Europe's access to space as the established leader in space transportation, satellite systems and services, Astrium has for over 40 years been dedicated to bring you all the space you need - now and in the future. It is a mission which resonates with many of the most prestigious names in space Ariane, the International Space Station, Envisat, Mars Express, Skynet 5. It is a mission with a consistent commitment, to offer our customers the best possible solutions in the market, with unbeatable levels of, quality, cost-efficiency and schedule adherence.

Astrium's technical excellence and extensive prime contractorship experience extend across all sectors of the space business launch vehicles, manned space activities and satellite systems and related services. Astrium operates via three branches:

c.1.1   Astrium Space Transportation

The European prime contractor for civil and military space transportation and manned space activities. It designs, develops and produces Ariane launchers and ballistic missiles for France's nuclear deterrent force, is industrial prime contractor for the Columbus laboratory and the ATV cargo vessel operating for the International Space Station, and is a specialist in atmospheric re-entry vehicles, propulsion systems and space equipment.

c.1.2   Astrium Satellites

A world leader in the design and manufacture of satellite systems, with business activities covering civil and military telecommunications and Earth observation, science and navigation programmes, together with a complete range of associated ground infrastructure and space equipment.

c.1.3   Astrium Services

The unique "one-stop-shop" in the worldwide satellite services market, with unrivalled capability and expertise in secure communications, Earth observation services, and navigation services.

C.2   ASTRIUM TOULOUSE

At its location in the southwest of France, Astrium in Toulouse specialises in satellite prime contracting, design, assembly integration and test for communications, Earth observation and science satellites. Its expertise also extends to avionics, optical instruments, on board software and ground systems at subsystem level. An additional and rapidly growing area of expertise is its services arm covering both global space-based communications solutions and sophisticated geo-information services.

LIST OF ACRONYMS

a	Acceleration
A	Matrix of energy influence coefficients
E_*	Total energy of the subsystem
$\mathbf{E}$	Vector of the total energy
F	Force
g	Acceleration in [g]
j, k	Index of the modes
L	Matrix of the damping loss factor
n	Index of a point in the subsystem
$N^{(*)}, N_p$	Number of points chosen in the subsystem
N_m	Number of modes in the bandwidth
m	Mass
M_r	Modal overlap
$M^{(*)}, M$	Mass of the subsystems
$P^{(*)}$	Power of the subsystem
P_*	Loss power of the subsystem
$\overline{P}_*$	Net power flow beetwen the subsystems
P_{in}	Input power
$\mathbf{P}_{in}$	Vector of input power
$\dot{q}$	Velocity
$\ddot{q}$	Acceleration
r, s	Index of the subsystems
S	Spectral density
T	Kinetic energy
v	Velocity
W	Input power
$\mathbf{W}$	Vector of input power
X	Inverse matrix of energy influence coefficients
α	modal receptance
α_*	Coefficient of the modal shape
Δ	Viscous damping
η	Damping loss factor

γ   Coefficient between the acceleration of the first and the third method
Γ   Cross modal power
ω   Frequency
Ω   Bandwidth
ϕ   Mode shape
ψ   Cross-mode participation factor
ρ   Density
ζ   Damping factor

BIBLIOGRAPHY

[1] N. Baldanzini. Progettazione meccanica per la riduzione del rumore e delle vibrazioni: lo strumento della statistical energy analysis. *XXX Convegno nazionale AIAS*, 2001. (Cited on pages 9 and 37.)

[2] Gerard Borello. Pyroshock modeling using virtual sea. 2008.

[3] Maxime Brel. Analyses vibroacoustiques de structures spatiales par la methode sea. Master's thesis, Institut Supérieur de Mécanique de Paris - Supméca, 2009. (Cited on page 15.)

[4] A. Carcaterra and A. Sestieri. Complex envelope displacment analysis: a quasi static approach to vibrations. *Journal of Sound and Vibration*, 1997. (Cited on page 8.)

[5] Benjamin Cimerman, Tej Bharj, and Gerard Borello. Overview of the experimental approach to statistical energy analysis. Vibro-Acoustic Sciences Inc. - Ford Motor Company - InterAC, –.

[6] Jacek F. Gieras, Chong Wang, and Joseph Cho Lai. *Noise of polyphase electric motors*, chapter 10 Statistical Energy Analysis. Taylor & Francis Group, 2006. (Cited on pages 7, 30, and 37.)

[7] F. Fahy and A.D. Mohammed. A study of uncertainty in applications of sea to coupled beam and plate systems. part 1: Computational experiments. *Journal of Sound and Vibration*, 1992. (Cited on page 24.)

[8] L. Gagliardini, L. Houillon, L. Petrinelli, and G. Borello. Virtual sea: mid-frequency structure-borne noise modeling based on finite element analysis. In *SAE Noise andVibration Conference*, 2003. (Cited on page 37.)

[9] Yan Harold, Perret Alan, and Nack Wayne. Statistical energy analysis by finite elements for middle frequency vibration. *Journal of Sound and Vibration*, 2000. (Cited on page 15.)

[10] A. J. Keane and W. G. Price. *Statistical Energy Analysis an overview, with applications in structural dynamics*. Cambridge university press, 1996. (Cited on page 3.)

[11] Takayuki Koizumi. *Vibration Damping, Control, and Design*, chapter 20 Statistical Energy Analysis. Taylor & Francis Group, 2007.

[12] R. Langley. A wave intensity technique for the analysis of high frequency vibrations. *Journal of Sound and Vibration*, 1992. (Cited on page 8.)

[13] R. Langley and P. Bremner. A hybrid method for the vibration analysis of complex structural-acoustic systems. *The Journal of the Acoustical Society of America*, 1999. (Cited on page 8.)

[14] A. Le Bot. Energy transfer for high frequencies in built-up structures. *Journal of Sound and Vibration*, 2002. (Cited on page 8.)

[15] R. H. Lyon and Maidanik. Power flow between linearly coupled oscillators. *The Journal of the Acoustical Society of America*, 1962. (Cited on page 3.)

[16] Richard H. Lyon. *Statistical Energy Analysis of dynamical system: theory and applications*. MIT press, 1975. (Cited on pages 3 and 34.)

[17] Richard H. Lyon and Richard G. De Jong. *Theory and applications of Statistical Energy Analysis*. RH Lyon Corp, 1998. (Cited on pages 3 and 34.)

[18] B. Mace. Shorter, energy flow models from finite element analysis. *Journal of Sound and Vibration*, 2000. (Cited on page 14.)

[19] B. Mace. Statistical energy analysis, energy distribution model and system modes. *Journal of Sound and Vibration*, 2003. (Cited on pages 7, 11, and 24.)

[20] B. Mace. Statistical energy analysis: coupling loss factors, indirect coupling and system modes. *Journal of Sound and Vibration*, 2005. (Cited on page 22.)

[21] B. Mace and A. N. Thite. *Statistical Energy Analysis: coupling loss factors, indirect coupling and system modes*. University of Southampton - Institute of Sound and Vibration Research, 2004. (Cited on page 11.)

[22] I. Moens. *On the use and the validity of the energy finite element method for high frequency vibrations*. PhD thesis, K.U.Leuven, 2001. (Cited on page 8.)

[23] G. Orefice, C. Cacciolati, and J. L. Guyader. The energetic mean mobility approach. In *IUTAM Symposium on SEA*, 1997. (Cited on page 8.)

[24] Ennes Sarraj. Energy-based vibroacoustics: Sea and beyond. Technical report, Gesellschaft für Akustikforschung Dresden mbH, –. (Cited on page 8.)

COLOPHON

This report was realized on LaTeX with the *ArsClassica* package developed by Lorenzo Pantieri. The package can be found in CTAN.